MUTATIONAL ANALYSIS OF THE LASSA VIRUS GLYCOPROTEIN HIGHLIGHTS REGIONS REQUIRED FOR RECEPTOR INTERACTION AND FUSION PROTEIN FUNCTION

by

JACOB ALSTON

(Under the Direction of Melinda Brindley)

ABSTRACT

Enveloped viruses utilize surface expressed glycoproteins in order to mediate both virus attachment and entry. The purpose of this work was to characterize the Lassa virus glycoprotein receptor binding (GP1) and fusion active (GP2) subunits, and to identify residues required for receptor interaction(s) and mediating viral-cell fusion. We biochemically evaluated 140 constructs containing mutations in either the GP1 or GP2 subunit. The constructs were assessed for their ability to mediate fusion, become processed and surface expressed, and transduce two well characterized haploid cell lines. Constructs harboring mutations within the GP1 subunit hypothesized to be inhibiting primary receptor alpha-dystroglycan (αDG) usage were also tested for protein-protein interaction. Our findings highlighted several amino acid residues required for αDG interaction and presumably lysosomal associated membrane protein 1 (LAMP1), a second Lassa virus receptor, interaction. We also identified residues mapping in or near GP2 functional domains that are required for protein function.

INDEX WORDS: Arenavirus, Lassa, Glycoprotein, Receptor Binding, Fusion

MUTATIONAL ANALYSIS OF THE LASSA VIRUS GLYCOPROTEIN HIGHLIGHTS REGIONS REQUIRED FOR RECEPTOR INTERACTION AND FUSION PROTEIN FUNCTION

by

JACOB ALSTON

BS, Appalachian State University, 2014

A Thesis Submitted to the Graduate Faculty of The University of Georgia in Partial Fulfillment of the Requirements for the Degree

MASTER OF SCIENCE

ATHENS, GEORGIA

2017

MUTATIONAL ANALYSIS OF THE LASSA VIRUS GLYCOPROTEIN HIGHLIGHTS REGIONS REQUIRED FOR RECEPTOR INTERACTION AND FUSION PROTEIN FUNCTION

by

JACOB ALSTON

Major Professor:	Melinda Brindley
Committee:	David Peterson
	Mark Tompkins

Electronic Version Approved:

Suzanne Barbour
Dean of the Graduate School
The University of Georgia
August 2017

DEDICATION

Dedicated to Susan Z. Alston, for her kindness and devotion, and for supporting me throughout my time at the University of Georgia.

ACKNOWLEDGEMENTS

I would like to express my appreciation to Dr. Melinda Brindley for her patience, knowledge, and support throughout my time as a graduate student at the University of Georgia; her mentorship has been instrumental. I also thank my committee members, Dr. David Peterson and Dr. Mark Tompkins, for their guidance throughout my research.

Finally, I thank my intermediate and extended family for their continuing care both at home and throughout my Master's research. Without them, none of this would have been possible. My parents, sister and wife have backed me through endless love and faith.

TABLE OF CONTENTS

CHAPTER 1

SPECIFIC AIMS

Arenaviruses are an emerging threat throughout Africa and the Americas. Many arenaviruses are capable of inducing hemorrhagic fever (HF) which causes classical symptoms including mucosal bleeding, respiratory distress, and shock. Human infection primarily occurs through contact with rodent reservoirs but can also occur via person-to-person contact. Currently there is no vaccine for any arenaviral pathogen and treatment relies on semi-efficacious measures. Both Ribavirin, a broadly acting anti-viral, and antibody therapy have been used to treat arenaviral infections; however, these treatments are associated with severe side effects and are only effective if used early in infection (1-3).

Numerous individuals worldwide are infected by arenaviruses each year. The Old World arenavirus, Lassa virus (LASV), infects hundreds of thousands annually with a documented case fatality rate of 1% (4). Due to the ease of transmission, lack of therapeutics, and mortality associated with infection, LASV is categorized as a class A pathogen (5).

The appearance and protein structure of viruses depend on its lifecycle. Upon budding from an infected host cell, the arenavirus particle is enveloped in a host membrane. In order to re-enter host cells, enveloped viruses encode viral glycoprotein(s) to interact with cellular receptor(s) and mediate fusion. The mature LASV glycoprotein (GP) exists as a trimer and is composed of three domains: the stable signal peptide (SSP), GP1, and GP2. Each domain is responsible for a functional step in virus entry. Lassa SSP is required for proper GP trafficking and pH sensing, GP1 is required for receptor binding, and GP2 is required for mediating fusion pore formation. Our goal was to identify regions within GP1 required for receptor interactions as well as regions within GP2 required for mediating protein function/fusion.

Specific Aim 1

To determine the regions within LASV GP1 required for alpha-dystroglycan interaction

Old World and New World clade C arenaviruses primarily utilize alpha-dystroglycan (αDG) to attach and enter cells. A second virus receptor in the lysosome, lysosomal associated membrane protein-1 (LAMP1), is specifically utilized by LASV for efficient cellular entry. We hypothesized that the αDG binding site is conserved among arenaviruses which utilize αDG for cellular entry. To identify specific regions within LASV GP1 responsible for αDG interactions, we utilized insertional mutagenesis, carbohydrate addition and subtractions, and alanine scanning of charged and hydrophobic amino acids. The mutated constructs were tested for protein expression, cleavage, fusion, transduction capability, and αDG binding. Data gained from these experiments showed that the αDG receptor binding site is located at the trimer interface and may span multiple GP1 monomers. These findings correlate with previously published data regarding LCMV- αDG interactions.

Specific Aim 2

To determine specific residues within LASV GP2 required for mediating protein function

Lassa virus GP2 is the fusion active subunit of the GPC and unlike conventional class 1 fusion proteins it contains both a fusion peptide and fusion loop. We hypothesized that both charged and hydrophobic residues play critical functional roles within GP2. To examine the amino acids necessary for fusion peptide functionality, GP2 reconfiguration, and fusion pore formation we utilized alanine scanning to mutate both hydrophobic and charged residues within the GP2 subunit. Constructs were tested for protein surface expression, processing, fusion and transduction capabilities using a Vesicular stomatitis virus (VSV) pseudotype system.

Information gained from these experiments highlighted residues involved in the fusion process. Future experiments will biochemically test where in the fusion processes the mutation affects.

Chapter 2

Arenavirus Disease and Entry Mechanisms: A Review

Global Impact

Viruses impact health around the world on a daily basis. Unfortunately, diseases caused by viruses do not often receive global attention until a large outbreak or spillover cases occur. The 2014 West Africa Ebola (EBOV) outbreak, which lasted approximately two years, showed how emerging infectious diseases can negatively impact daily life. By the end of the outbreak, nearly 28,000 individuals were infected by EBOV which attributed to over 11,000 deaths (6). The size and escalation of the outbreak prompted a quick research response around the world. In the United States alone, roughly 2.8 billion dollars was spent on EBOV research and aid to better understand how the virus functions and to prevent infection (6). Ultimately, EBOV research led to advancements in vaccine development and therapeutics which helped to mitigate the outbreak (7, 8).

Apart from EBOV, the arenavirus family contains many emerging pathogens endemic to Africa and the Americas. There are five arenaviral species endemic to South America and one endemic to Africa associated with hemorrhagic fever. Lassa fever virus is the most predominant arenavirus in Africa, and serology suggests that there are hundreds of thousands of infections per year (9). Lassa virus is capable of causing hemorrhagic fever in humans, and is spread through close contact with rodent hosts or infected individuals (10, 11). The first identified LASV host was *Mastomys natalensis,* and in 2016 two other rodent reservoirs, *Hylomyscus pamfi* and *Mastomys erythroleucus,* were identified in West Africa (12, 13). Identification of multiple LASV hosts is significant because it could permit the maintenance of the virus in more demographic regions.

Current predictions state there will be a doubling of LASV infections by 2050 which is due to the discovery of multiple rodent hosts and the current trend in global climate change allowing for more ecological niches.

Although LASV is endemic to West Africa, globalization and world travel result in imported cases around the world. There have been documented cases of LASV in Germany, Sweden, the United Kingdom and the United States (14-17). In 2015, a man contracted LASV in West Africa before traveling back to the US and died from the disease after being treated in New Jersey. No known reservoirs for LASV exist outside of West Africa, but the disease has potential to spread through person-to-person contact. Therefore, a better understanding of the virus is needed for the future development of both therapeutics and vaccines.

Virus Entry Mechanisms

Virus entry is the first step of the infectious process. Surface expressed cellular proteins and sugars act as receptors to anchor viral particles to the membrane. Viruses encased in a host derived membrane encode receptor binding and fusion competent proteins to overcome lipid membrane boundaries. Activation of the fusion subunit releases the viral genome into the cell for replication. The location of the viral fusion event is specific to the virus but can occur either at the cell surface or throughout the endocytic pathway.

Common forms of virus entry include clathrin mediated endocytosis (CME), caveolin-dependent endocytosis and macropinocytosis. Clathrin polymerization and accessory proteins create invaginations in the cellular membrane which ultimately undergo membrane scission by dynamin. This process creates an endosomal vesicle in the cell cytoplasm which is trafficked to target membranes (18). Caveolin, similar to clathrin, also coats endocytic vesicles and helps to

drive vesicle formation (19). Many viruses utilize CME for entry including the semliki forest virus and vesicular stomatitis virus (VSV) (20, 21), while viruses such as SV40 exploit caveolar vesicles for efficient cellular entry (22).

Unlike clathrin and caveolar dependent endocytosis, macropinocytosis is nonspecific (23). Under normal physiological conditions, macropinocytosis is used by the cell to uptake fluids/small molecules and is driven largely by actin rearrangement at the cell membrane. Although unspecific, many viruses are able to hijack this pathway for internalization (23). Once endocytosed, the virus containing vesicles are trafficked to a late endosome or endo-lysosome. Viruses that utilize this pathway are able to mediate fusion pore formation at low-pH.

Lassa virus is able to enter cells through macropinocytosis and entry is largely independent of clathrin and caveolin mediated endocytic pathways (24-26). This mechanism of uptake is unlike the natural ligand of αDG, laminin, which is endocytosed in a dynamin dependent process (27). After receptor interactions at the cell surface, the LASV particle is endocytosed and trafficked to a late-endosome. Cellular factors involved in the uptake of LASV particles include actin rearrangement, Cdc42 activation and activation of the sodium-hydrogen exchange which are all hallmarks of macropinocytosis (25). Interestingly LASV does not induce membrane ruffling/blebbing to the extent seen with other viruses utilizing macropinocytosis for entry (25, 26). By not causing extensive morphological changes at the cell membrane, the virus may be better adept to avoid immune surveillance. Once the LASV containing vesicle fuses with a lysosome, genome release is mediated through low-pH activation of the fusion subunit. The LASV receptor interactions and fusion event will be discussed in the following sections.

Lassa Virus Particle Description

Viruses are one of the smallest infectious agents known, and contain either a DNA or RNA genome which encode viral proteins. LASV is an enveloped virus consisting of a bi-segmented, negative sense, single stranded RNA genome in ambisense orientation. Both RNA segments, known as the large and small segment, encode two proteins. The large segment encodes both the matrix (Z) protein and polymerase (L) while the short segment encodes for the nucleoprotein (NP) and glycoprotein complex (GPC). All four proteins are required for a replication competent virus; however, VLP formation can occur with solely expressing Z protein (28).

When viewed with electron microscopy, the arenavirus particle appears sandy and harbors mature GP trimers imbedded in the viral membrane. The sandy appearance is due to the incorporation of host ribosomes; however, this phenomenon does not enhance virus replication (29). The GPs expressed on the viral surface enable LASV to bind host receptors, gain entry and mediate fusion pore formation resulting in genome release. Particles void of glycoprotein are not able to infect host cells.

Viral Glycoprotein Processing and Structure

Viral glycoproteins can be grouped into three classes. Each class shares commonalities in the structure and function of the glycoprotein, as well as how the fusion pore is activated and formed. LASV GPC is a class I fusion protein, and will be discussed at length. During replication, viral glycoproteins that are considered class I are produced as precursors and must undergo proteolytic cleavage to carry out viral functions. Without the cleavage/priming event, the precursor glycoprotein is unable to function properly (30). This step is critical for the infectivity of future progeny.

Class I viral glycoproteins undergo proteolytic cleavage at various time points of infectivity; before, during or after viral egress. The cleavage event is carried out by host cell proteases to create a mature form of the glycoprotein from the glycoprotein precursor. Several Class I proteins have been extensively studied in regards to processing. For example, the HIV envelope protein is produced in the ER and cleaved by cellular signal peptidases to produce gp160. Then, proteolytic cleavage of the HIV-1 gp160 precursor occurs intracellularly by subtillisin family proteases, including both furin and LPC/PC7 (31, 32). This cleavage results in two subunits, gp120 and gp41, responsible for host cell binding and fusion pore formation respectively. Without gp160 processing, HIV-1 is unable to elicit cellular entry.

Like HIV, Influenza virus HA must undergo proteolytic cleavage to mediate virus attachment and entry. Influenza HA0 is processed by host cell proteases to form the HA1 and HA2 subunits. Many proteases, including trypsin-like, subtillisin-like and serine member proteases have been identified to support the processing of HA0 (33-35). The cleavage site for HA0 is dependent on the strain of influenza, and the enzyme cleaves HA0 is dependent on the amino acid architecture. For instance, furin recognizes a polybasic cleavage site found in some avian HA proteins while other HA cleavage sites harbor monobasic sequences (36). Unlike HIV, where gp160 is processed in the infected cells, the processing event for influenza HA can occur in the host cell, at the cell membrane or on mature viral particles.

The paramyxovirus fusion protein, F, requires proteolytic processing for functionality (30). Many paramyxovirus F proteins encode a polybasic cleavage site and are processed intracellularly by host furin proteases (33). Viruses that do not encode the furin cleavage site (R-X-K/R-R) may

be cleaved by other host proteases such as cathepsins or trypsin-like proteases (37-39). Without protein processing, paramyxovirus F protein is unable to mediate virus-cell fusion.

Like the other Class I proteins above, the LASV glycoprotein complex (GPC) is first synthesized as a precursor protein, GPC, which undergoes two cleavage evens (Fig 2.1). The first processing event occurs in the ER by a host cell signal peptidase cleaving the LASV SPP, and the second processing event occurs in the cis-Golgi by SKI-1/S1P producing the receptor binding and fusion active subunits (40-43). Unlike other class I fusion proteins, the relatively long signal peptide in arenaviruses is not degraded; it remains stable and serves a chaperone-like function which is necessary for the correct protein processing, trafficking, and pH sensing/activation (44-46).

Structure of the Lassa Virus Glycoprotein

The LASV glycoprotein is expressed as a trimeric complex imbedded in the viral envelope (Fig 2.1). As stated previously, the mature trimeric GP complex can be divided into three domains: GP1, GP2 and the SSP. Each domain is responsible for a major function in viral entry and their structure will be discussed in detail.

The LASV SSP is an essential subunit in the mature glycoprotein and has multiple functions within the LASV lifecycle. Sequence analysis of the arenaviral SSP reveals an N terminal myristolation motif, two hydrophobic transmembrane domains, and a zinc finger binding motif which secures an interaction with GP2. Membrane topology studies confirmed the orientation of the SSP in the lipid bilayer. The arenaviral SSP positions both the N- and C-terminus intracellularly, crosses the membrane twice and contains a small ectodomain (47). Mutational analysis within the SSP reveals several key residues required for GPC trafficking and pH sensing.

Specifically, interruption of a conserved K33 residue expressed in the ectodomain inhibits GP fusion (48). Deviation from a charged residue at position K33 reduces fusion, so it is thought that the conserved lysine residue may assist to destabilize the fusion active subunit under low-pH conditions. Other studies show that SSP-GP2 interaction is necessary for proper protein trafficking, and mutations to the zinc finger binding domain result in impaired glycoprotein trafficking (49). In general, the SSP functions as a key subunit within the arenaviral GP assisting in protein trafficking, folding and fusion.

A majority of the GP mass is composed of the GP1 and GP2 subunits. In the mature GP, the GP1 and GP2 subunits interact non-covalently and mediate both receptor interactions and fusion. Both the neutral and low-pH conformations of LASV GP1 have been crystalized (50, 51). Comparison of the two crystals highlight structural rearrangements that occur within GP1 at low-pH. The LASV histidine triad undergoes major rearrangements at low-pH which may help to destabilize the GP1 trimer organization and release from GP2 (50, 51). A second conformational difference seen comparing GP1 at neutral and low-pH is the position of the termini. At neutral pH, the N-terminus of GP1 forms a beta strand and interacts with a second beta strand located in GP2 (50). The low-pH GP1 monomer positions both the N- and C-termini facing upwards away from where the GP2 subunit would be located (51). Overall, the flexibility within the GP1 subunit may allow for the disengagement of GP1 from GP2 and result in membrane fusion.

In addition to the crystallization studies, the LASV GP has been viewed with cryo-electron tomography at various pH conditions. Structural changes within the GP occur when the pH is lowered below 7, and at a pH of 3 the GP1 subunit disassociates from GP2 (52). This finding

correlates with the previous crystal structures suggesting that both GP1 and GP2 undergo conformational changes under low-pH.

The LASV GP2 subunit has only recently been crystalized in the pre-fusion form and has not been crystalized in the post-fusion form (50). However, due to the highly conserved GP2 sequence/structure between LASV and LCMV, we can utilize the pre- and post-fusion LCMV crystal structures for characterization (53, 54). Both LASV and LCMV are categorized as a Class I fusion protein and consist of two heptad repeat (HR) domains, an N-terminal fusion peptide, and an internal fusion loop. Each domain is required for the transition of pre-fusion GP2 to post-fusion GP2. Specifically, the hydrophobic fusion loop and fusion peptide insert into the host membrane upon GP2 activation. This event creates a bridge between the viral and host membranes. To close the gap and mediate fusion pore formation, HR1 and HR2 undergo structural rearrangements which lead to membrane merger. Taken together, all three arenaviral GP subunits function as a unit to permit proper GP processing/folding, trafficking, internalization, and fusion allowing for viral replication.

Virus Receptor Interactions

Enveloped viruses have evolved many mechanisms to accomplish membrane fusion and genome delivery. Some virus such as paramyxoviruses, bind to the host cell and fuse at the cell surface, whereas other viruses, including influenza, utilize cellar endocytosis machinery to be delivered deeper in the cytoplasm where fusion is triggered by low-pH. In each case, the first step in infection is attachment to the cellular membrane.

LASV entry requires a two-step process in which the GP undergoes a pH induced receptor switch (Fig 2.2). Lassa GP1 first interacts with its primary receptor, αDG, expressed on the cell

surface (55). In cells lacking αDG, LASV is able to utilize other entry factors including heparan sulfates, DC-SIGN and TAM family member proteins (56-58). Although LASV can use alternative methods of entry, the most efficient virus uptake occurs through primary receptor usage.

The receptor binding domain within LASV GP1, required for αDG interaction, has not been identified. However, the αDG binding site required for LASV attachment has been extensively characterized. Interaction between LASV GP1 and αDG requires the expression of a specific o-mannosyl group on αDG (59). In cells lacking LARGE, the glycosyltransferase necessary for the o-mannosyl modification, LASV is unable to efficiently enter (59). Bound to αDG on the outer membrane, LASV is thought to become endocytosed through the macropinocytosis pathway described earlier (24, 25, 58). Once in the macropinosome/endosome LASV is trafficked until lysosomal merger, and acidification of the endo-lysosome compartment causes conformational changes to occur within GP1. Similar to HIV gp120 conformational changes allowing for co-receptor binding, the pH induced changes in LASV GP1 reduces affinity for αDG and increases affinity for LAMP1 (58, 60, 61). The second receptor for LASV, LAMP1, was identified using a haploid screen in cells deficient in dystroglycan (58). Several other proteins involved in trafficking, sugar structure and protein modifications were also identified. One identified protein, ST3GAL4, involved in modifying complex N-glycans led the researchers to mutate N-glycosylation motifs in the LAMP1 sequence. Interruption of a LAMP1 N-glycan motif at position N76 impaired receptor interactions suggesting that this sugar structure is involved in receptor binding (58).

The location of the LAMP1 binding site within GP1 is currently being investigated in the field. Ron Diskin's group has shown that the LASV GP1-LAMP1 interaction occurs through a

conserved histidine triad (H92-H93 and H230), and that mutations to the histidine triad reduce LAMP1 binding (51). The histidine triad is conserved between LASV and LCMV; however, previous studies have shown that LCMV does not bind to LAMP1 nor is LAMP1 required for entry (62). This suggests that either mutations to the LASV GP1 histidine triad alter protein folding or the histidine triad of LASV/LCMV GP1 assume different conformations. Cryo-electron tomography images of LASV GP1 show that under low-pH the GP1 trimer undergoes conformational changes and exposes a LAMP1 binding groove located between monomers (52). In accordance to Diskin's group, the histidine triad is oriented within the putative LAMP1 binding groove. This data suggests that the histidine residues are either directly involved in LAMP1 interaction or involved in GP1 conformational changes that indirectly affect LAMP1 binding (51, 52).

Although activation of the LASV GP can occur with low-pH alone (52, 63), the GP1-LAMP1 interaction is hypothesized to lower the activation energy needed to overcome GP triggering (64). It is believed that protonation of the histidine triad leads to fusion activation. Assuming the surface-exposed residue H230 is protonated first, this would increase the energy needed to protonate the two nearby adjacent histidine residues (H92-H93). To overcome energy boundaries, LAMP1 may supply a negative charge to the histidine triad under acidic conditions. This would allow the charge of the microenvironment to become net neutral and may permit the further protonation of H92-H93 (64). Ultimately, protonation of the histidine triad is thought to act as a switch inducing conformational changes within GP1 leading to GP2 triggering. To support this hypothesis, a negative charge at position H230 both inhibits GP1-LAMP1 interaction and

allows for the early activation of LASV GP at a higher than optimal pH (64). Overall, the LAMP1 receptor interaction leads to the efficient activation of the fusion protein and enhances virus entry.

Class I Virus Fusion Proteins

All enveloped viruses encode proteins responsible for carrying out fusion pore formation. The basic composition of a Class I fusion protein consists of two heptad repeats, a fusion peptide, transmembrane domain, and cytoplasmic tail. Pre-fusion structures of Class I fusion proteins vary between viral families; however, all Class I fusion proteins exist as trimers in both the pre and post-fusion forms. The triggering event which mediates the transition from the pre-fusion to post-fusion glycoprotein form virus specific and includes receptor binding, low-pH, and receptor binding plus low-pH.

Following the activation of a Class I fusion protein, the fusion peptide is inserted into the host cell membrane. Once a sufficient number of fusion proteins trigger and overcome the metastable hairpin conformation, fusion will proceed. The hairpin folds back on itself in an energetically favorable conformation and forms a six helix bundle mediated by the N- and C-terminal heptad repeat domains (6HB). During the process of re-folding an intermediate state, known as hemi-fusion occurs. Hemifusion is defined as the merger of the outer host membrane to the outer viral membranes. Full collapse of the viral glycoprotein overcomes the hemifusion intermediate and allows for fusion pore formation (Fig 2.3) (65). Establishment of the fusion pore is needed for viral genome release.

The GP2 subunit of LASV and other arenaviruses is responsible for mediating fusion between the viral and host cell membranes. The protein structure of GP2 resembles that of a class one fusion protein, but the fusion domain resembles a hybrid structure containing both an internal

fusion loop and an N terminal fusion peptide (53). The fusion peptide of LASV GP closely resembles that of PIV5 F while the fusion loop resembles Ebola GP and other class II/III fusion proteins (66). Both the fusion peptide and fusion loop work together to anchor GP2 into the host membrane leading to fusion pore formation.

To understand the transition fusion proteins undergo when activated, the pre-fusion LASV and post-fusion LCMV GP2 crystal structures will be compared (Fig 2.4). The amino acid sequence similarity and protein structure between LASV and LCMV GP2 closely correlate. When activated, the arenaviral GP2 subunit must undergo drastic conformational changes to mediate fusion pore formation. In the pre-fusion state, the GP1 and GP2 subunits are in contact with one another and share considerable surface area (Fig 2.4). The N-terminal fusion peptide is buried between the GP1 and GP2 subunit interface. The heptad repeat regions, which facilitate 6HB formation, are less structured compared to the post-fusion form. Heptad repeat 1 (HR1) is divided into four separate domains in the pre-fusion state; three of four domains within HR1 create separate alpha helixes and one domain is unstructured. While the HR2 domain interacts with b-sheets within the T-loop as well as the N-terminus of GP2 (54). Overall, the pre-fusion structure of GP2 is seemingly more compact and unstructured compared to the post-fusion structure.

The introduction of low-pH causes major conformational changes to occur within LCMV and LASV GP (53, 54). In the post-fusion state, GP1 disassociates from the GP trimer. Heptad repeat-1 forms a continuous α-helix, not seen in the pre-fusion state, and positions the N-terminal fusion peptide and internal fusion loop to be inserted into the host membrane. Once a sufficient number of GP triggering events have occurred to overcome membrane energy barriers, the extended GP2 conformation folds back on itself to form a pre-bundle complex. The pre-bundle

conformation brings the host and viral membranes in close proximity. Collapse of the pre-bundle conformation results in 6HB and hemi-fusion to occur. In the 6HB conformation, HR1 and HR2 make several contacts and full collapse of the GP2 subunit allows for fusion pore formation to occur. The formation of a fusion pore releases the viral genome into the cytoplasm for viral replication.

Small Molecule Inhibitors

Several viral inhibitors have been developed that help reduce disease burden felt by HIV, Influenza and many other viruses. These inhibitors are designed to block virus replication at critical points throughout their lifecycle. Effectively blocking the virus lifecycle leads to lower titers in the host and helps to clear infection. Inhibitors identified for HIV include both antibodies and peptides which bind to the glycoprotein and inhibit virus entry (67, 68). Currently there is only one fusion inhibitor, Fuzeon (T-20), used in the clinic to treat HIV-1. The peptide T-20 is derived from the C terminal heptad repeat of gp41 and blocks HIV entry by inhibiting 6HB formation (69-72). Blocking 6HB results in the inhibition of fusion pore formation which leads to lower viral infection. A second promising HIV entry inhibitor, LP-19, works in a similar mechanism as Fuzeon. When comparing LP-19 to T-20, LP-19 blocks HIV-1 entry with greater efficiency and is more potent at lower concentrations (73). However, unlike Fuzeon, LP-19 has not undergone clinical trials.

Severe cases of influenza can also be treated with viral inhibitors. There are currently four viral inhibitors on the market which impede Influenza virus replication. Two inhibitors, Amantadine and Rimantadine, act against the M2 proton channel and inhibit viral un-coating. Two other inhibitors, oseltamivir and zanamivir, inhibit Influenza NA required for viral egress. Other

inhibitors exist in the lab setting and include sialic acid like inhibitors and antibodies. These inhibitors block virus entry by binding near the sialic acid binding domain within influenza HA (74) (75-77).

Although there are no licensed viral inhibitors, besides ribavirin, used for arenaviral treatment, several have been identified in a lab setting. Many of the identified arenaviral inhibitors block pH induced glycoprotein activation. A recently developed small peptide derived from Pichinde virus HR-N, AVP-p, blocks entry of several arenaviruses through early triggering of the arenavirus glycoprotein (78). Early activation of the viral glycoprotein results in reduced viral infectivity. Other arenaviral inhibitors have been identified via high throughput screening. Specifically ST-193, 16G8 and 17D1 reduce LASV GP medicated entry and are shown to be inhibiting low-pH conformational changes (79-81). The primary region thought to be targeted by the inhibitors is the SSP and GP2 interface (79). The SSP-GP2 interaction is required for multiple GP protein functions including protein trafficking, pH sensing and fusion. Therefore, blocking the SSP-GP2 interface would impair normal GP functions and result in less virus entry.

In order to design future arenaviral inhibitors, a basic understanding of the viral entry proteins is needed. The work presented here sought to better define micro domains within the LASV GP1 and GP2 subunit required for receptor interaction(s) and fusion respectively. To identify the aDG receptor binding site within LASV GP1 and functional domains within GP2 we utilized site directed insertional and point mutagenesis. Data gained from these studies highlights amino acid residues required receptor interaction and GP2 function.

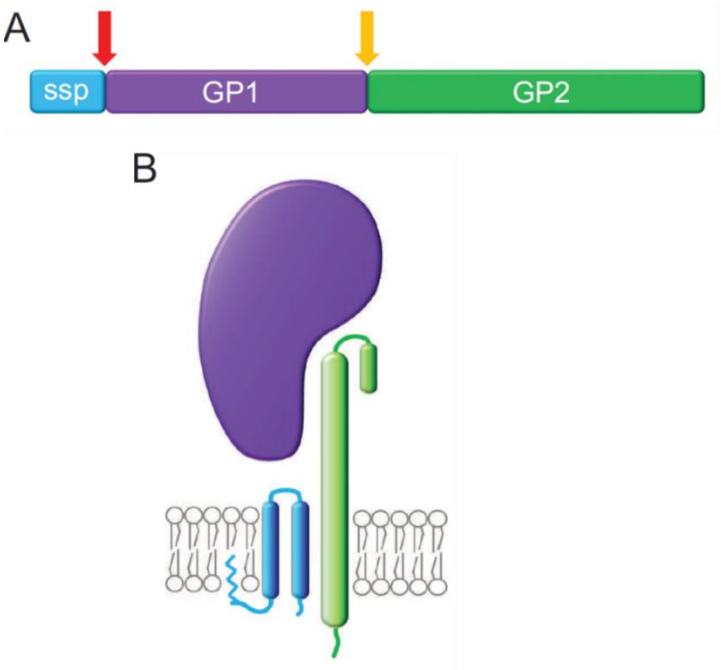

Figure 2.1. The subunits and structure of the Lassa virus glycoprotein complex. (A) The LASV glycoprotein complex consists of the membrane-integrated stable signal peptide (SSP) (blue), GP1 subunit (purple) and the non-covalently attached GP2 subunit (green). The GPC is cleaved by signal peptidase (red arrow) and SKI-1/S1P (yellow arrow) during protein processing. (B) Cartoon of the SSP, GP1 and GP2 heterotimer complex in the lipid bilayer.

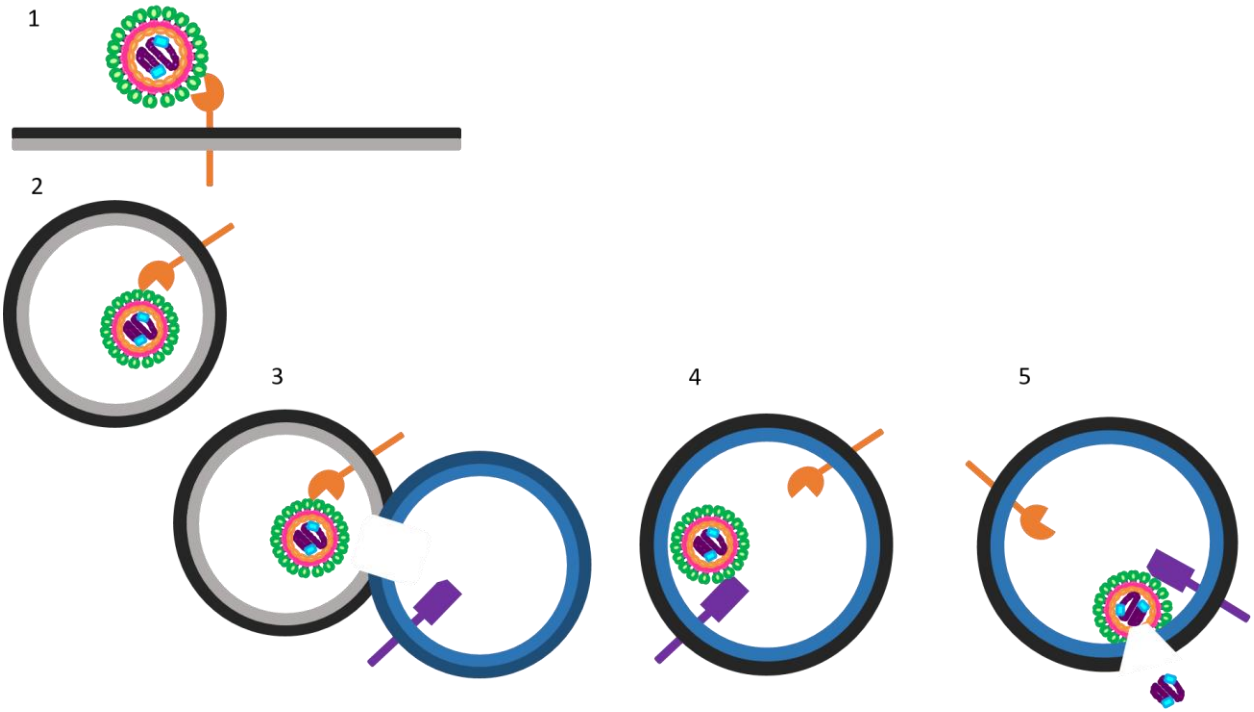

Figure 2.2. LASV Enters Cells via Macropinocytosis and Undergoes a Receptor Switch to Mediate Efficient Cellular Entry. (1) Lassa virus binds to αDG expressed on the outer cell membrane and is endocytosed by micropinocytosis. (2-3) Upon macropinosome maturation the vesicle fuses with a lysosome. The LASV GP undergoes a receptor switch when exposed to low-pH in the lysosomal environment; losing affinity for αDG and gaining affinity for LAMP1. (4-5) Low-pH along with LAMP1 binding activates the LASV GP2 fusion protein and allows for fusion pore formation. The opening of a fusion pore releases the LASV genome into the cell cytoplasm for replication.

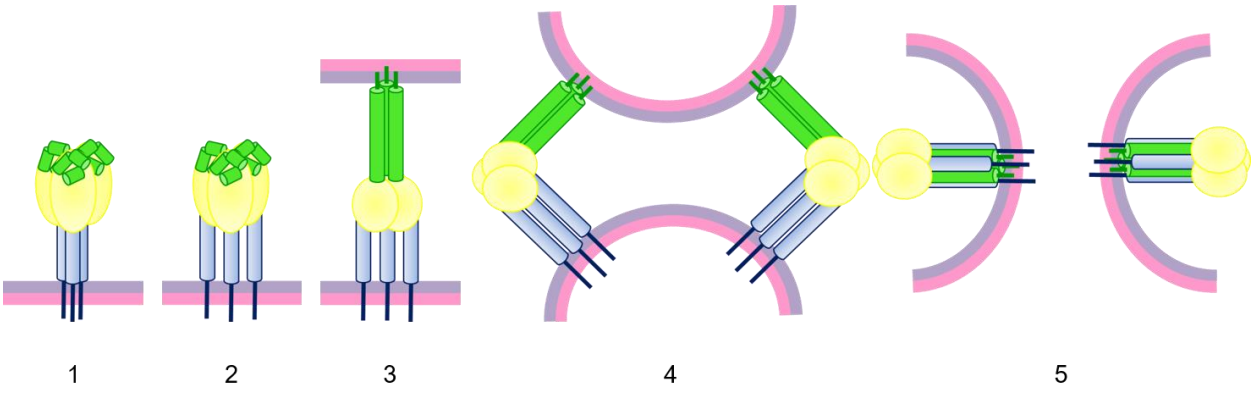

Figure 2.3. Class I membrane fusion pathway. The steps leading from Class I fusion protein activation to mediating fusion pore formation. (i-ii) The viral glycoprotein, expressing a receptor binding domain and a fusion active subunit, undergoes a triggering event. (iii) An extended prehairpin conformation forms following the glycoprotein triggering event. (iv) To overcome the energy needed for membrane merger, multiple viral glycoproteins are needed to tigger. These triggering events lead to a cluster of hairpins. Prebundle formation brings the host and viral membranes in close apposition. (v) 6HB formation drives the hemifusion event, which mediates the merger of the outer viral envelope and host membrane (not shown). After hemifusion, full collapse of the viral glycoprotein occurs and results in fusion pore formation.

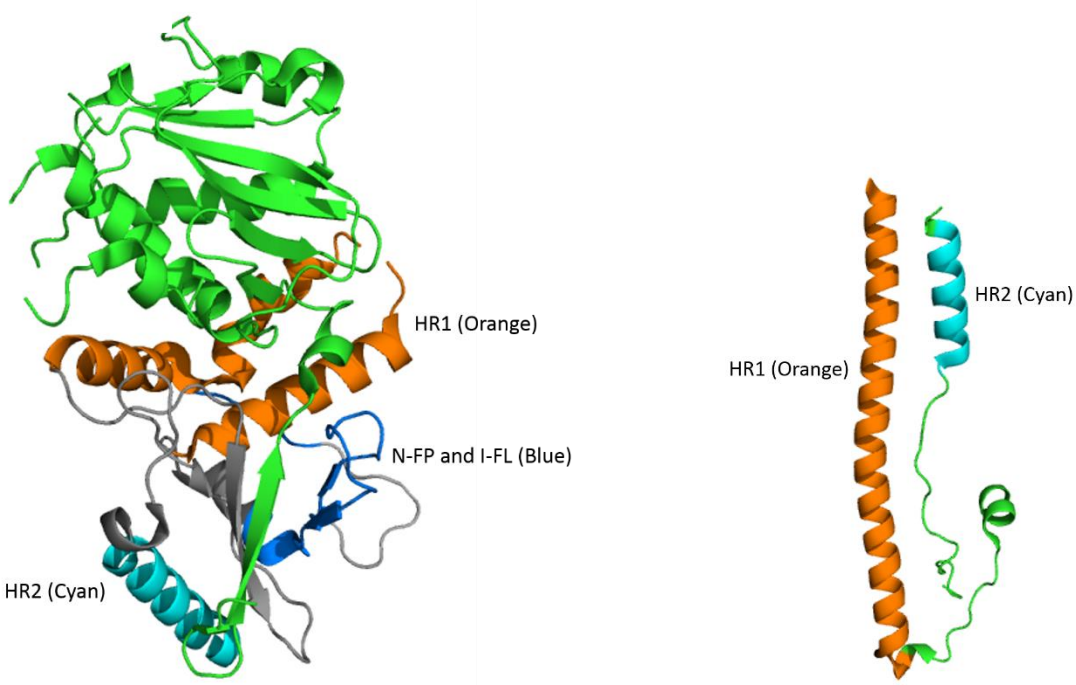

Figure 2.4. Structural Differences Between LASV/LCMV Pre-Fusion and Post-Fusion Conformations. The LASV fusion protein undergoes major confomrational changes when exposed to low-pH. (left) Under neutral pH, LASV GP2 shares a large amount of surface area with the receptor binding GP1 subunit and the domains required for mediating viral-host membrane fusion are seemingly unstructured to the post-fusion structure (right). After activation, the HR1 domains makes a continuous alpha-helix and interacts with HR2 to mediate 6HB and fusion pore formation.

CHAPTER 3

MUTATIONAL ANALYSIS OF LASSA VIRUS GLYCOPROTEIN HIGHLIGHTS REGIONS REQUIRED FOR ALPHA-DYSTROGLYCAN UTILIZATION

Introduction and Objectives

Lassa fever is a hemorrhagic disease caused by an Old World arenavirus known as Lassa virus (LASV). The virus was first isolated in Nigeria in 1969 and is currently endemic in West Africa (82). Serological studies suggest hundreds of thousands of people are infected each year (9). While most infections are mild or asymptomatic, 15-20% of cases require hospitalization and result in approximately 5000 deaths annually (83-85). The rodent host for LASV is the multimammate rat, *Mastomys natalenis* (13). Recently, the virus has been isolated from *Hylomyscus pamfi* and *Mastomys erythroleucus*, potentially increasing its geographic range (12). Human exposure occurs through direct contact with the infected rodents, rodent excrement, or close contact with infected patients (10). Due to the high morbidity and mortality associated with Lassa hemorrhagic fever, LASV is classified as a category A pathogen (86).

Lassa virus is an enveloped ambisense RNA virus with a bi-segmented genome. Viral particles are covered in mature glycoprotein (GP) trimeric spikes, which mediate viral entry. Like other class 1 viral fusion proteins, the envelope glycoprotein precursor (GPC) is translated as a single polypeptide and is proteolytically cleaved into three subunits. Processing occurs first in the ER by a cellular signal peptidase. GPC is then trafficked to the cis-Golgi and processed by cellular proprotein convertase subtilisin kexin isozyme-1/site-1 protease (SKI-1/S1P) to produce a non-covalent stable signal peptide SSP/GP1/GP2 hetero-trimer (Fig 3.1 A-B) (40-43). Unlike other class I fusion proteins, the relatively long signal peptide of GPC is not degraded; it serves a

chaperone-like function necessary for the correct trafficking and processing of GP (44, 46, 87). SSP interacts with the cytoplasmic domain of GP2 and is involved in pH sensing (48, 49, 88). GP1 is responsible for binding to cellular receptors (55, 58), while GP2 mediates membrane fusion during viral entry (53, 54, 89).

Cellular entry of LASV is a multistep process involving multiple GP1-receptor interactions. First, GP1 interacts with a cell surface receptor on the plasma membrane, mainly alpha-dystroglycan (αDG) (55). Additional surface receptors can mediate LASV entry in the absence of αDG, including heparin sulfate, DC-SIGN and TAM family members (56-58). This initial GP1-receptor interaction induces viral internalization through a clathrin, caveolin, and dynamin independent process (24, 25, 58). Once within the low-pH environment of the endo-lysosomal compartment, GP undergoes conformational changes that reduce its affinity for αDG and increase its affinity to a second receptor, lysosomal associated membrane protein 1 (LAMP1) (60, 61). Engagement of LAMP1 by LASV GP1 is hypothesized to lower the activation energy needed to mediate GP2 conformational changes that fuse the viral and cellular membranes, completing the entry pathway (52).

Previous studies have provided new structural information for both the pre-fusion conformation and pH-induced changes in the LASV glycoprotein. Recently, the trimeric pre-fusion GP1/GP2 crystal of LASV was solved (50). This structure provides novel insight into the LASV GP complex including trimer organization, glycosylation, and potential receptor binding sites. The LASV GP1 monomeric protein was previously crystalized under low-pH conditions (pH 5) (51). The low-pH purified protein was unable to interact with αDG, but interacted with LAMP1, suggesting that the crystal structure resembles GP1 in the lysosome (51). Comparison of the pre-

fusion GP1 crystal (isolated at pH 8) and the pH 5 GP1 crystal structure highlights several low-pH-induced conformational changes required for LAMP-1 interactions (50).

In addition to the crystallization studies, a cryo-electron tomography (cryo-ET) study was able to construct three-dimensional structures of LASV GP trimers under increasingly acidic pH conditions (pH 7, 5, and 3) (52). Tomographic reconstructions suggest the GP1 subunit undergoes conformational changes at pH 5, opening a putative LAMP1 binding crevice at the GP1 trimeric interface (51, 52). Pseudoatomic models fit both pre-fusion GP1/GP2 and low-pH GP1 crystal structures into the low resolution cryo-ET densities, providing three-dimensional models of GP trimer organization (50-53).

LASV entry is most efficient when GP1 interacts with αDG and LAMP1. While the GP1 binding interface has been mapped in both αDG and LAMP1, the corresponding receptor-binding sites in GP1 have yet to be elucidated. Utilizing the new crystal structure as a model, we used carbohydrate shielding, insertional mutagenesis, and alanine scanning mutagenesis to identify regions within GP1 important for receptor interactions (Fig 3.1D). Previous data suggests that the LASV GP must be in a trimeric form to interact with αDG. We hypothesize that the receptor biding domain involves at least two GP1 monomers and is located in the central trimeric core.

Materials and Methods

Cell lines and transfections. Vero (African green monkey kidney) cells stably expressing human SLAM were maintained in Dulbecco's modified Eagle's medium (DMEM) supplemented with 5% (vol/vol) fetal bovine serum (FBS) at 37°C and 5% CO_2 (90). HAP1 and HAP1-ΔDAG1 cells (Horizon Discovery) were maintained in Iscove's media supplemented with 10% (vol/vol) FBS at

37°C and 5% CO_2. All transient transfections were performed using GeneJuice (Millipore) as per manufacturer's instructions.

Molecular biology. The LASV GPC protein coding sequence was codon optimized for mammalian expression and cloned into a pcDNA3.1intron vector. Gene expression was initiated by a CMV promotor and the β-globin intron was engineered in the 5' untranslated region (UTR) to increase protein production. A carboxy-terminal 3xFLAG tag was added to the cytoplasmic tail of the GP2 subunit for biochemical detection. HA tag coding sequence (YPYDVPDYA) was added to the plasmid at the indicated locations using PCR-based insertional mutagenesis with Q5 polymerase (NEB). Point mutations were introduced with QuikChange mutagenesis and PfuTurbo-HS polymerase (Agilent). The plasmid DNA of each construct was sequenced, and the presence of each mutation was confirmed. Complete sequence information is available upon request.

Surface biotinylation. Vero cells were transfected with plasmid DNA encoding the indicated Lassa GPC mutants. Thirty-six hours following transfection, cells were washed with cold PBS and biotinylated with 0.5 mg/mL sulfosuccinimidyl-2-(biotinamido) ethyl-1,3-dithiopropionate (Thermo) for 30 min on ice. The reaction was quenched using Tris-HCl, and cells were lysed in M2 lysis buffer (50 mM Tris, pH 7.4, 150 mM NaCl, 1 mM EDTA, 1% Triton X-100) at 4°C and clarified with centrifugation (20,000xg, 15 min). Lysate was incubated with streptavidin sepharose beads (GE Healthcare) for 60 min while rotating. Following incubation, the streptavidin sepharose beads were washed in buffer 1 (100 mM Tris (91), 500 mM lithium chloride, 0.1% Triton X-100) and then in buffer 2 (20 mM HEPES [pH 7.2], 2 mM EGTA, 10 mM magnesium chloride, 0.1% Triton X-100), incubated in urea buffer (200 mM Tris, pH 6.8, 8 M urea, 5% sodium dodecyl

sulfate [SDS], 0.1 mM EDTA, 0.03% bromophenol blue, 1.5% dithiothreitol) for 30 min at 55°C, and subjected to immunoblot analysis.

Antibodies and immunoblots. Surface biotinylated material was fractionated by gel electrophoresis on 10% Tris-glycine gels (ThermoFisher) and transferred to polyvinylidene difluoride (PVDF) membranes (GE Healthcare). GP was detected with specific antibodies directed against the Flag epitope tag (M2; Sigma). Immunoblots were developed using mouse IgG horseradish peroxidase (HRP)-conjugated secondary antibodies (Jackson) and a ChemiDoc digital imaging system (Bio-Rad). Each experiment was repeated at least three independent times and a representative image is shown. Trichloroacetic acid (TCA) precipitated pseudotyped particles were fractionated as described for biotinylated material. Protein was detected with specific antibodies directed against LASV GP2 (22.5D), kindly provided by Dr. James Robinson (Tulane University), and against VSV matrix (23H12, courtesy of Dr. Douglas Lyles; Kerafast) (92, 93). Alpha dystroglycan was detected with IIH6 monoclonal antibody (EMD Millipore). Immunoblots were developed using HRP-conjugated human IgG and mouse IgG (Jackson) secondary antibodies, respectively, and a ChemiDoc digital imaging system (Bio-Rad). Immunoblots were quantified using ImageLab software.

Cell-to-cell fusion assay. Vero cells were co-transfected with Lassa GP mutants and pmaxGFP (4:1 ratio). Forty hours following transfection, media was removed and replaced with DPBS (pH 4) and incubated (37°C and 5% CO_2) for 30 min to allow glycoprotein triggering. The DPBS was replaced with DMEM and cells were incubated for an additional 3 hours to enable membrane rearrangement and clear syncytia formation. Four representative pictures of the fusion were taken

using the Zoe microscope (Bio-Rad) (20x magnification) and unfused cells were counted. Quantification of fusion was calculated using the following equation:

$$Fusion = \frac{(unfused\ cells\ in\ mock\ transfected - unfused\ cells\ in\ mutant\ transfected)}{(unfused\ cells\ in\ mock\ transfected - unfused\ cells\ in\ WT\ GPC\ transfected)} \times 100$$

Each mutant was assessed in the fusion assay in three independent experiments.

VSV pseudotype production and transductions. GP constructs lacking the c-terminal 3xFlag tag were used to make the vesicular stomatitis virus (VSV) pseudotyped particles. Vero cells were transfected with LASV GP DNA. Thirty-six hours following transfection the cells were transduced with VSVΔG-GFP particles pseudotyped with VSV-G (MOI 1) for one hour (courtesy of Dr. Michael Whitt; KeraFAST) (94). The particle-containing media was then replaced with fresh DMEM. VSVΔG-GFP particles displaying the LASV GP were collected 12 hours following the transduction. These particles were applied onto HAP1 and HAP1-ΔDAG1 cells in volumes of 0.25 mL and 1 mL, respectively. A higher volume of particles was used to transduce HAP1- ΔDAG1 cells in order to overcome the decreased transduction efficiency when the cells are missing the primary receptor (58). The number of GFP positive cells was enumerated in a flow cytometer. Results are displayed as the percent of GFP positive cells present in a population of 10,000 live cell events compared to GP wild-type transduction. To monitor GP incorporation onto the VSV particles, 1 mL of pre-cleared VSV transduction particles were precipitated using 10% wt/vol TCA. The TCA treated proteins were pelleted (20,000xg, 30 min, 4°C), washed with acetone, dried, and denatured using SDS-Urea buffer (200 mM Tris, pH 6.8, 8 M urea, 5% sodium dodecyl sulfate [SDS], 0.1 mM EDTA, 0.03% bromophenol blue). Particles were subjected to immunoblot analysis for both VSV matrix levels and incorporated GP2.

Co-immunoprecipitation. Sheep polyclonal anti-human dystroglycan antibodies (R&D Systems) were bound to protein G beads (BioRad) and incubated with αDG purified from rabbit muscle (95). The prepared beads were then divided equally into VSV pseudotyped particles containing a normalized about of GP and incubated for 1 hour. Protein complexes were precipitated and washed three times with PBS. Bound proteins were eluted by incubating beads with urea-SDS plus DTT, heat denatured (56°C for 30 min), and separated on SDS-PAGE. Immunoblot analysis examined the amount of precipitated αDG and associated GP2.

Results

With the overarching goal of understanding the functional and spatial organization of the arenavirus pre-fusion glycoprotein structure, we utilized the trimeric GP pre-fusion crystal structure (50) to identify residues involved in receptor interactions.

Function of GPC N-Linked Glycans

Arenavirus GP N-linked glycans play significant biochemical roles in virus-cell interactions (96, 97). Previous studies found that specific N-linked glycans in LCMV GP1 were necessary for GP trafficking, fusion activity, and infectivity (96). LASV GP1 contains seven conserved N-linked glycosylation sites. Removing glycans at positions 81, 91, 101, and 121 was previously shown to inhibit GPC processing into GP1 and GP2 (97), although receptor binding and fusion activity were not evaluated. We reproduced the seven N-glycan mutants by changing glycosylation site motifs from N-X-S/T to N-X-A. To examine the level of processed GP on the cell surface, surface proteins were biotinylated, concentrated using streptavidin sepharose beads, and subjected to immunoblot analysis (Fig 3.2A). All mutated GP's migrated faster than parental GP, confirming that all seven sites are glycosylated. We similarly found that removing the N-

linked sites at T81 and S91 resulted in GPC processing defects (Fig 3.2A and C). However, we found the remaining five N-glycan mutations result in detectable levels of GP1-GP2 processing, including T101 and S121. Our use of a codon optimized expression construct and examining surface material 36 hours after transfection, rather than 24, may have enabled T101A and S121A to reach a detectable steady state levels of processed GP1-GP2 at the cell surface (97).

To determine if the constructs lacking N-glycans produce functional GP, we determined if they could produce syncytia, or multinucleated cells, in a cell-to-cell based fusion assay. Incubating LASV GP transfected cells with a low-pH buffer results in efficient GP activation and results in robust syncytia formation (Fig 3.2B). By comparing the extent of syncytium formation between mutant and parental GP, we can determine the fusion efficiency of each mutant. The fusion activity of the N-glycan mutants closely correlated with the cleavage efficiency (Fig 3.2C), suggesting the glycans are not required for productive cell-to-cell fusion.

Cell-to-cell fusion assays do not completely recapitulate the process that occurs when a viral particle fuses with an endosomal membrane. Virus-to-cell entry requires the viral glycoprotein to facilitate interactions with cellular receptors to initiate endocytosis. Once trafficking to the proper cellular compartment occurs, LASV virus must undergo a receptor switch in the endo-lysosome before membrane fusion. In order to determine if the GP1 constructs can mediate viral entry, VSV pseudotyped particles were produced containing LASV GP on their surface. Particle transduction was monitored in two haploid cell lines, HAP1 and HAP1-ΔDAG1. LASV entry into HAP1 cells and HAP1-ΔDAG1, a cell line deficient in αDG, has been thoroughly documented by recent genetic screens (58, 59). Gene-trap screening of HAP1 cells re-confirmed LASV GP's interaction with properly glycosylated αDG significantly enhances cell entry (59). A

second gene-trap screen in HAP1-ΔDAG1 cells identified an additional, lysosomal receptor, LAMP1 (58). Because efficient HAP1 entry of LASV occurs through αDG interactions, and HAP1-ΔDAG1 cell entry occurs through other cell surface receptors, such as heparin sulfate receptors (58), we propose that constructs exclusively demonstrating reduced transduction efficiency into HAP1 cells are inefficiently engaging αDG. In order to demonstrate the entry enhancement by αDG, we added the same volume of pseudotyped particles coated with LASV GP on both cell lines (Fig 3.2D). LASV GP entry into HAP1 cells produced 8.4 ± 0.83 times more GFP positive cells than the same volume of particles added to HAP1-ΔDAG1 cells. To compensate for the decreased entry into HAP1-ΔDAG1 cells, we increased the volume of particles used to transduce this cell type. When examining the transduction efficiencies, each mutant was compared to parental GP in each cell type. Therefor specific defects in HAP1 cell entry would highlight mutations that facilitated viral uptake through αDG interactions.

Because GP can only fuse if GP1-GP2 processing occurs, we examined transduction efficiency for constructs with at least 50% cleavage efficiency. Five glycosylation removal GP1 constructs were examined in transduction assays, T101A, S111A, S121A, S169A and T226A. All five constructs efficiently transduced both cell types, suggesting GP missing a single N-glycan retains cell entry (Fig 3.2E).

Engineering N-linked glycosylation sites onto GP1

Carbohydrate shielding, or glycosylation site additions, can be used to map glycoprotein structural domains (98-100). We engineered seven additional glycosylation sites throughout GP1 (Fig 3.3). All glycosylation sites were predicted to be present on the surface of the GP1 model, although H141N, N148S, V187T, and Y253N had potential to impede trimer formation based on

the new trimeric structure (32). The mutants were evaluated for the incorporation of the glycan, as well as processing with surface biotinylation assays (Fig 3.3A). Glycosylation additions were confirmed by the slower mobility pattern of GP1-GP2 on an immunoblot compared to parental GP, which was observed for mutants H141N, V187T, D211S, and Q232N (Fig 3.3A). The remaining constructs K116S, N148S, and Y253N were not glycosylated, suggesting these motifs were not recognized by cellular glycotransferases. The trimeric structure predicts N148 and Y253 to be located at the center of the trimer, possibly making these residues inaccessible. K116 was also not glycosylated, despite its predicted location on top of the trimer with clear access to glycotransferases. The natural glycosylation site at N119 may sterically prevent neighboring glycan additions.

Cleavage was reduced for all glycosylated constructs except for D211S, indicating the additional glycans reduced SKI-1/S1P recognition or efficient GP trafficking to the Golgi in most cases. Cell-to-cell fusion activity was proportional to cleavage efficiency, suggesting the additional glycans did not prevent GP2 activation at low-pH if GP1-GP2 processing occurred (Fig 3.3B). Although Y253N did not appear to be glycosylated, the mutation decreased fusion relative to the amount of cleaved GP suggesting that the point mutation alone may decrease the efficiency of GP refolding and completing the fusion process.

Transduction assays were performed with K116S, N148S, D211S, and Y253N, which demonstrated >50% GP processing (Fig 3.3C). Both D211S and Y253N reduced transduction compared to parental GP, yet transduction levels between HAP1 and HAP1-ΔDAG1 cells were similar. This suggests mutations were not altering interactions with αDG, but inhibiting an entry step common in both cell types. The Y253 construct's reduced fusion activity may account for

reduced transduction levels, while the additional glycan on D211S may have decreased transduction efficiency in both cell lines.

Characterization of GP1 using insertional mutagenesis

Few of the additional N-linked glycosylation sites that we engineered were efficiently glycosylated (Fig 3.3). Therefore we employed insertional mutagenesis to add bulky epitope tags throughout GP1 to impede receptor binding (Fig 3.4). The nine amino acid HA epitope tag (YPYDVPDYA) was inserted at 21 positions along the length of GP1. Insertion sites were chosen to avoid perturbation or disruption of protein tertiary structures. To increase the flexibility of the HA tag, 14 insertions included Gly-Gly-Ser linkers (lHA) flanking the insertion.

Surface expression of HA insertion constructs varied. Most constructs were produced, but the majority of insertions resulted in processing defects, evidenced by the lack of cleaved GP2 in surface biotinylated material (Fig 3.4A). Although the HA insertion sites were added to unstructured surface loops, the insertions appeared to alter protein folding in the majority of the constructs, preventing GPC processing by SKI-1/S1P. Overall, only seven of the twenty-one mutants displayed appreciable cleavage compared to parental GP (Fig 3.4A).

To test for GP fusion activity, the mutant constructs were expressed in Vero cells and incubated with a low-pH buffer to trigger conformational changes. As expected, mutations that inhibited GPC cleavage did not display any fusion activity (Fig 3.4B). Constructs that retained GPC processing all produced syncytia, suggesting the HA insertions did not prevent the low-pH conformational changes when SKI-1/S1P recognition occurred (Fig 3.4B).

Transductions were carried out for seven of the 21 insertion constructs. Only one construct, 61HA, was able to transduce both cell lines (Fig 3.4C). The GP1/GP2 crystal structure found the N-terminal region of GP1 produces an extended β-sheet that interacts with GP2 (32) (Fig 3.1D). Therefore, the HA epitope tag addition after residue 61 would be near the viral membrane and separated from main body of GP1. Three constructs, 146HA, 227HA and 250HA, were able to transduce HAP1-ΔDAG1 cells but were unable to efficiently transduce HAP1 cells, suggesting that these insertions inhibit αDG utilization (Fig 3.4C). As expected, HAP1 transduction was not completely eliminated. Lassa entry into HAP1 can occur through an alternative pathway that does not require αDG (58, 59). Therefore, particles that have reduced affinity for αDG may still be able to enter HAP1 cells through the alternative, albeit less efficient pathway. The remaining three constructs; 150HA, 172HA and 230HA showed low to no transduction in both HAP1 cell lines, suggesting the inserts inhibited a step in the entry process that is in common between both cell lines, such as LAMP1 interaction (Fig 3.4C).

Alanine scanning of hydrophobic and charged residues

Large insertions and glycan additions tended to block GP cleavage, preventing full GP characterization. To increase the chances of producing GP trimers that are trafficked to the cell surface in a processed state, we introduced single amino acid substitutions. Hydrophobic and charged residues can be critical for virus glycoprotein-receptor interactions and entry (91, 101-104). To locate possible αDG binding sites in LASV GP1, alanine scanning was used to mutate conserved hydrophobic and charged residues. Out of 16 hydrophobic mutants, 11 demonstrated more than a 50% reduction in cleavage efficiency, and/or fusion activity compared to parental GP (Fig 3.5 A-B). Several of the hydrophobic residues were located in secondary structures of GP1,

and presumably alanine substitutions resulted in protein misfolding. For the remaining mutants, those that produced cleaved GP2 were able to form syncytia. The L133A mutant produced little protein, and along with the decreased cleavage efficiency (60% of parental GP), resulted in very low fusion activity.

Six hydrophobic mutants were examined in transduction assays. The majority of the hydrophobic mutations transduced both cell lines as well as wild-type GP (Fig 3.5C). The low protein level seen with L133A did not significantly impact transduction efficiency. While F147A was able to transduce HAP1-ΔDAG1 cells at a similar level as wild-type GP, transduction in HAP1 cells was reduced to 42%. The transduction defect in HAP1 cells with no defect in HAP1 ΔDAG1 cells suggests F147 is important for efficient αDG utilization.

Fourteen conserved charged residues were mutated to alanine, including a described histidine triad (H92, H93, and H230), which has been implicated in LAMP1 interaction (51, 61). All mutated GPs were cleaved and transported to the cell membrane at levels greater than 60% of parental GP (Fig 3.6A). The charged residue mutants also displayed high levels of cell-to-cell fusion activity (Fig 3.6B). Only GP mutant R248A-R250A demonstrated reduced fusion.

We produced VSV pseudoparticles expressing all fourteen charged mutations and tested their ability to transduce HAP1 and HAP1-ΔDAG1 cells (Fig 3.6C). Mutant H92A-H93A was unable to transduce either cell type tested. H230A, the third residue of the described histidine triad, showed relatively high levels of transduction. Mutants K125A-K126A, H141A, and R248A-R250A demonstrated a reduced transduction in HAP1 cells compared to HAP1-ΔDAG1 cells. Although transduction into HAP1 cells was not completely inhibited, the data suggest the mutations may decrease efficient interaction with αDG.

Additional Targeted Mutations

The transduction data suggested residues located near the center of the GP1 trimer were key for efficient αDG entry. To more fully examine this region, an additional fifteen point mutations were created that focused on the regions surrounding the top of the GP1 trimer and residues adjacent to mutations that reduced transduction in HAP1 cells (Fig 3.7). To determine if combining some of the individual mutations that modestly decreased HAP1 entry would synergistically eliminate αDG binding, two double mutants that incorporated mutations at GP residues 141 and 147 were made. Constructs H92Y-H93Y and H230Y were also made to compare the effects of alanine versus tyrosine substitutions and to reproduce similar constructs tested in the study by Cohen-Dvashi et al (51, 61). Overall, surface expression and processing of the additional targeted mutants were near wild-type LASV GP levels with the exception of H92Y-H93Y and H141N-F147A. Both of these double mutants were produced but were poorly processed (Fig 3.7A). When the asparagine at position H141 in the double mutant was changed to alanine, surface expression, processing, and fusion increased. Histidines at position 92 and 93, when changed to alanines, retain processing and fusion activity (Fig 3.6B), but tyrosine substitution lead to GPC processing defects (Fig 3.7A). Previous work by Cohen-Dvashi et al tested individual mutations H92Y, H93Y, and H230Y for processing, surface expression, and fusion activity (61). When they individually changed each histidine to tyrosine, they found a reduction in the level of cleaved, surface expressed GP, but no significant changes in cell-to-cell fusion. Our double mutant, H92Y-H93Y, completely inhibited GP processing as well as fusion (Fig 3.7A and B). Similar to the previous study, H230Y was efficiently processed and induced cell-to-cell fusion at levels greater

than wild-type GP. In general fusion activity, with the exception of A177S, again closely correlated with cleavage efficiency (Fig 3.7B).

Of the 15 constructs made, 13 were tested in transduction assays. Only two constructs; Y150A and H141A/F147A showed reduced transduction in HAP1 cells compared to HAP1-ΔDAG1 cells (Figure 3.7C). The combination of H141A and F147A had an additive effect. Individual changes dropped HAP1 transduction to 40% of parental GP, and the double mutant dropped HAP1 transduction to 10% of parental GP while retaining near wild-type levels of HAP1-ΔDAG1 transduction. All other constructs were able to transduce HAP1 and HAP1-ΔDAG1 cells with similar efficiencies (Fig 3.7C). While H230Y did not result in cell type specific transduction defects, this mutation moderately reduced transduction in both cell lines, similar to the previous study (61).

GP incorporation onto VSV particles

While many of the constructs produced particles that transduced both cell types, some constructs did not efficiently transduce either cell line, or displayed a deficiency in a specific cell type. To ensure the low transducing constructs incorporated sufficient levels GP on the particle, immunoblots were performed (Fig 3.8). All particles incorporated the mutated GP constructs, including those constructs that failed to transduce both cell lines. K125A-K126A and Y150A, two mutants that demonstrated a reduction in HAP1 transduction and an enhancement in HAP1-ΔDAG1 cells, were consistently found on VSV particles at higher levels than wild-type GP. Similarly, R248-R250A was found on particles at a higher rate that parental GP, although it did not transduce better than wild-type.

Residues H141-F147 and R248-R250 are critical for αDG interaction

In order to directly assess the ability of GP mutants to bind with αDG, we performed a co-immunoprecipitation experiment. Beads coated with αDG were incubated with VSV pseudotyped particles containing either parental or mutant GP. We examined GP-H141A-F147A and GP-R248A-R250A, because they each contained point mutations that resulted in HAP1 entry defects. In addition, we evaluated GP-H230Y, a construct implicated in LAMP1 binding. Parental GP and GP-H230Y were efficiently precipitated by αDG, whereas we were unable to biochemically detect GP-H141A-F147A and GP-R248A-R250A (Fig 3.9A). This data further supports our conclusions that the central core of GP mediates interaction with αDG (Fig 3.9B).

Discussion

Here we provide data highlighting LASV GP1 residues important for receptor interactions. We produced and characterized a library of 80 constructs. Transduction was monitored in cell lines that differentially express the LASV receptor αDG. Biochemical characterization grouped GP1 mutants into various categories based on their transduction phenotypes (Table 3.1). The data implicate regions of GP1 that facilitate entry through αDG, as well as residues involved with LAMP1 interaction.

We tested all of the constructs in cell-to-cell fusion assays, and those that were efficiently processed, in pseudotype particle entry assays. A number of mutants including, H92A-H93A, 150lHA, 172HA, and 230lHA, produced large syncytia in cell-to-cell fusion assays, yet were unable to facilitate entry when incorporated onto VSV particles. This suggests the requirements for cell-to-cell fusion and virus-to-cell fusion are different. The luminal pH of most lysosomes ranges from 4.5-5 (105). In contrast, we utilized PBS at pH 4 in the cell-to-cell fusion assay

because this pH produced the most syncytia (data not shown and (106, 107)). We speculate LAMP1 may facilitate fusion pore formation at a more alkaline pH, thereby increasing the efficiency of LASV entry (61). The fusion assay may be able to circumvent the LAMP1 requirement with a more acidic environment, triggering fusion pore formation without LAMP1 interaction. This would explain why mutants can produce large syncytia when exogenous low pH buffer is added, yet are unable to productively enter cells on a pseudotyped particle. Removal of LAMP1 from cells dramatically decreases LASV entry efficiency, but does not eliminate it (58). Perhaps some virions encounter lysosomes with lower pH ranges, and the extra acidic environment overcomes the LAMP1 requirement similar to the cell-to-cell fusion assay.

LASV entry requires interactions with both cell surface receptors and an internal receptor, LAMP1 (58). As previously mentioned, we identified a number of constructs that blocked entry into both cell types tested: H92A-H93A, 150lHA, 172HA, and 230lHA. Both H92-H93 and H230 have been previously implicated in GP1-LAMP1 interaction (51). Protonation of the histidine residues may facilitate conformational changes that expose the LAMP1 binding site (61), which cryo-ET reconstructions suggest occurs in grooves between GP1 monomers that form under low-pH conditions (52). While histidines at positions 92, 93, and 230 may facilitate the low-pH conformational changes, 150lHA and 172HA fall on the opposite face of the crystal structure. If LAMP1 binding is occurring in a low-pH induced groove, both 150lHA and 172HA may sterically prevent LAMP1 binding, or cause premature shedding of GP1 from the glycoprotein complex. We did not identify any individual point mutations that prevented entry into both cell lines that were not previously associated with inducing low-pH conformational changes, suggesting further work is required to locate the specific residues directly involved in LAMP1 interaction.

While most constructs efficiently entered both cell lines, those containing mutations between amino acids 141-150 and 248-250 of GP1 demonstrated reduced transduction in HAP1 cells expressing αDG. A co-immunoprecipitation using VSV pseudotyped particles confirmed the role of residues H141, F147, R248, and R250 in direct αDG binding. Residues H141, N146, F147, and Y150 face the three-fold axis of the trimer, forming a putative receptor binding site (Fig 3.9B, shown in red). A similar region within LCMV has been implicated in LCMV GP1-αDG interaction (53). Previous biochemical studies show OW arenavirus monomeric GP1 is unable to interact with αDG, which supports a binding site that requires an intact trimer (51, 53, 58). Residues R248 and R250 also face this center axis, but are located deeper in the core (Fig 3.9B, shown in orange). Presumably, αDG would not be interacting with the buried center of the trimer, but removal of the charged residues may alter the conformation of the domain above. K125A-K126A and 227HA modestly reduced HAP1 transduction and are located further away from the trimeric center. These mutations may exert long-range conformational changes that alter the αDG binding site (Fig 9B, shown in yellow). For example, K125 and K126 line the GP1-GP1 interface within the trimer, and therefore may play a role in maintaining the center conformation.

In 2015, the largest screen of LASV genomes revealed that isolates are highly heterogeneous and group by geographic distribution (108). The GP1 subunit had the highest sequence diversity of the four viral proteins, presumably due to continuous immune selection. When comparing the GP1 subunit among the 180 sequences collected, 68% of the amino acid sequence was conserved. However, the regions we identified in this study that mediate αDG entry were 98-100% conserved, suggesting these residues are important for the structure or function of GP1. The few residues that differed contained conservative amino acid substitutions. Several

additional Old World arenaviruses including LCMV, Mopeia (MOPV), and Mobala (MOBV) use αDG as their primary surface receptor (109). A GP1 sequence alignment of these four viruses reveals the regions we identified in LASV-αDG engagement are similar among these Old World arenaviruses (Fig 3.9C). Furthermore, LCMV shares 63% sequence identity with LASV, and similar regions on GP1 have been implicated in LCMV's GP1-αDG binding site (53). Five residues have been identified which enhance LCMV GP1 binding to αDG; H136, S153, Y155, R190, and L260 (53, 110-114). Residues S153, Y155, R190, and L260 are located in the same region on GP1 that faces the three-fold trimer axis (53), further supporting this region's importance in αDG binding.

In summary, our data suggests that the αDG binding site on LASV GP1 is found at the top central core of the GP trimer. These data correlate with the hypothesized αDG binding regions within LCMV GP1 (53). Our data supports the hypothesis that the histidine triad plays a role in the pH conformational changes required for LAMP1 interaction. In addition, we identify two HA insertion mutants, 150HA and 172HA, that may sterically block LAMP1 binding. Knowledge gained by this study will aid the development of small molecule inhibitors to block LASV entry through its receptors αDG and LAMP1.

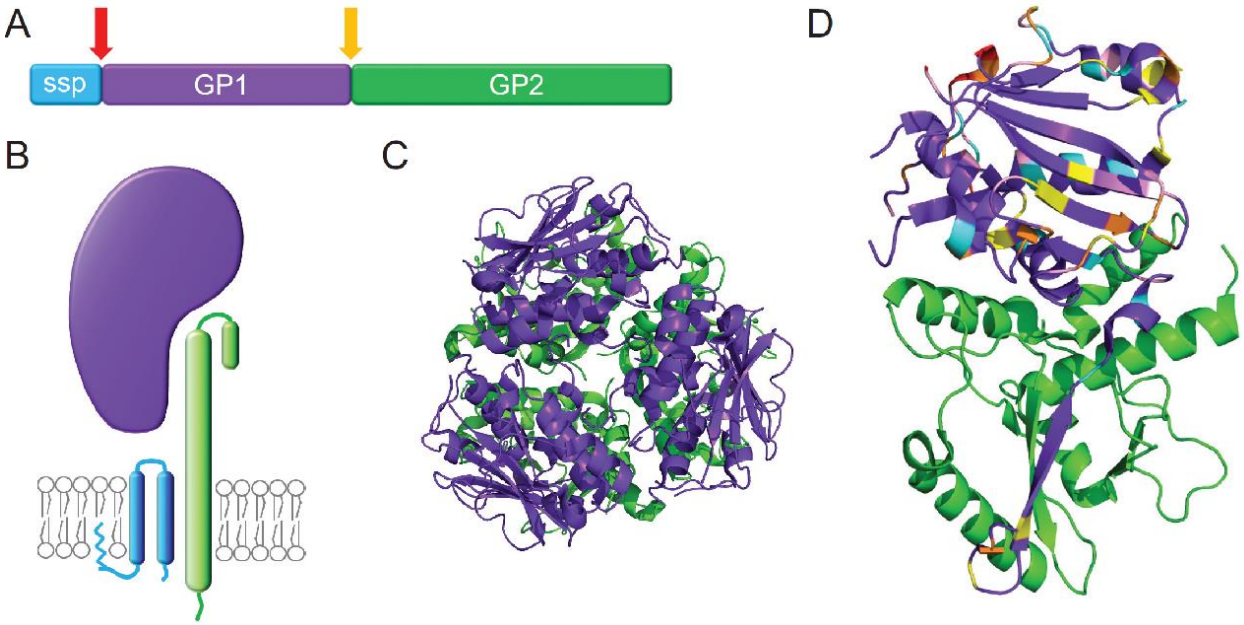

Figure 3.1. The subunits and structure of the Lassa virus glycoprotein complex. (A) The LASV glycoprotein complex consists of the membrane-integrated stable signal peptide (SSP) (blue), GP1 subunit (purple) and the non-covalently attached GP2 subunit (green). The GPC is cleaved by signal peptidase (red arrow) and SKI-1/S1P (yellow arrow) during protein processing. (B) Cartoon of the SSP, GP1 and GP2 heterotrimer complex in the lipid bilayer. (C) Trimeric LASV GP1-GP2 crystal structure, top down view, GP1 is in purple and GP2 in green (PDB 5vk2) (50). (D) The LASV GP1-GP2 crystal structure, side view, (PDB 5vk2) The engineered GP1 constructs are color-coded as follows: glycosylation site removals and additions (pink); HA-tagged sites (orange), alanine scanning of charged residues (yellow), alanine scanning of hydrophobic residues (blue), additional targeted residues (red). Note many of the targeted residues were found in regions of the structure that did not crystalize. All structures were rendered with PyMol.

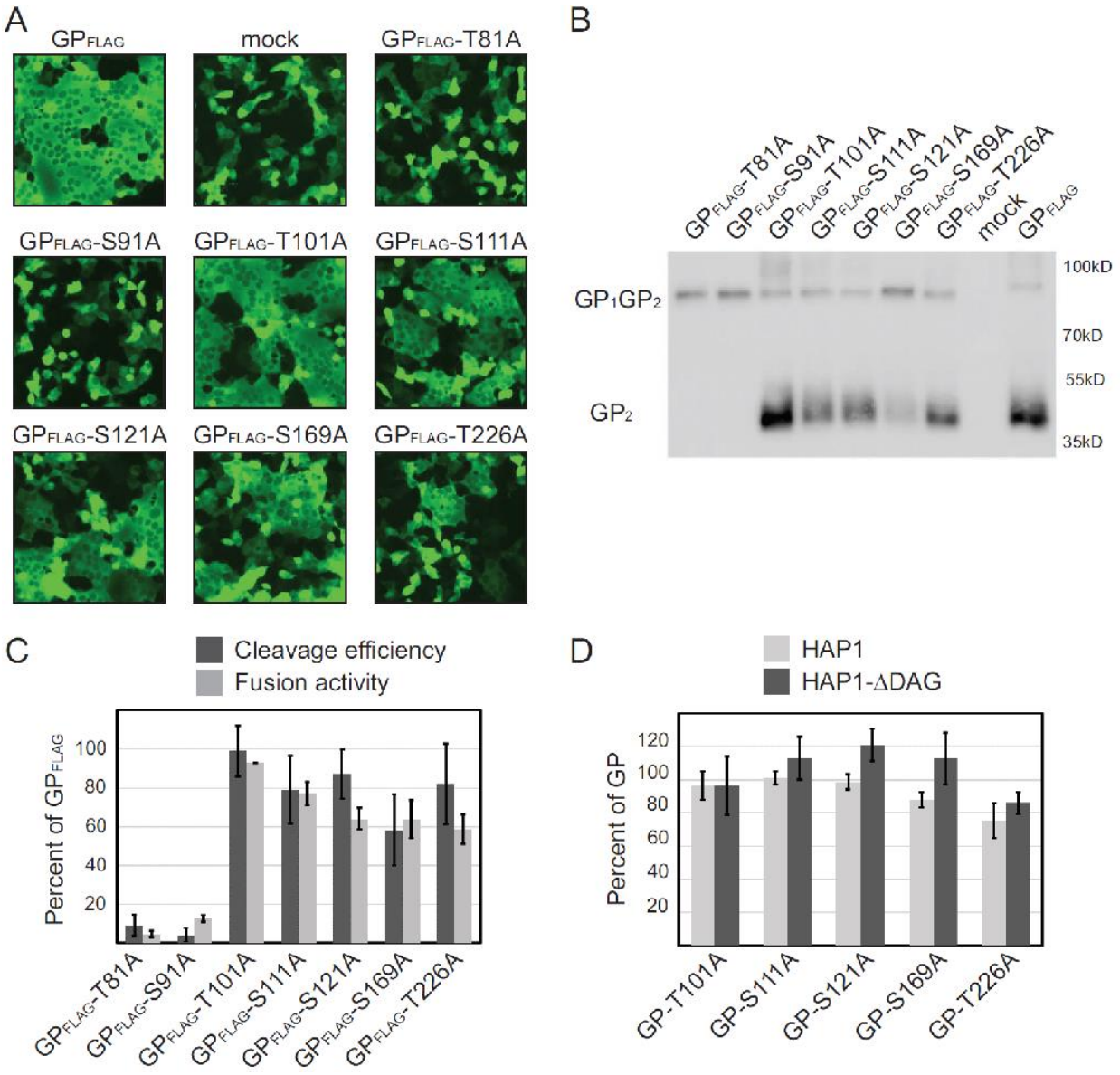

Figure 3.2. Processing and functional characteristics of surface-expressed GP1 N-glycosylation sites. (A) Vero cells were transfected with the indicated FLAG-tagged LASV GP variant or negative control. After 36 hours, cells were subjected to surface biotinylation. Surface expressed biotinylated proteins were concentrated using streptavidin sepharose beads. Precipitated proteins were separated by SDS-PAGE. Immunoblots were carried out to detect LASV GP surface expressed protein using an anti-FLAG antibody, M2. Immunoblot is a representative of four trials.

(B) Microphotographs of Vero cells co-transfected with plasmid DNA encoding LASV GP construct and GFP. Cell-to-cell fusion was assessed 3 h following low-pH media shock; magnification ×20. Representative fields of view are shown. (C) Fusion data for each construct was quantified via counting unfused cells and comparing to mock transfected wells. Quantified fusion data for each construct was normalized to LASV wt-GPC-3xFLAG. Cleavage efficiency was normalized to FLAG tagged GP using densitometry analysis. (D) Parental GP transduction efficiency in HAP1 and HAP1-ΔDAG1 cells. VSVΔG-GFP pseudo-particles containing LASV GP were added to both cells and the number of GFP positive cells were enumerated in a flow cytometer. The percentage of the cell population that was GFP positive is shown. (E) VSVΔG-GFP pseudo-particles containing LASV GP or N-glycosylation mutants were used to transduce HAP1 and HAP1-ΔDAG1 cells. The number of GFP positive cells were enumerated in a flow cytometer. Transduction efficiencies were normalized to parental LASV GP particle transduction values in each respective cell type. All data are based on the average and standard error of the mean of at least three replicate experiments.

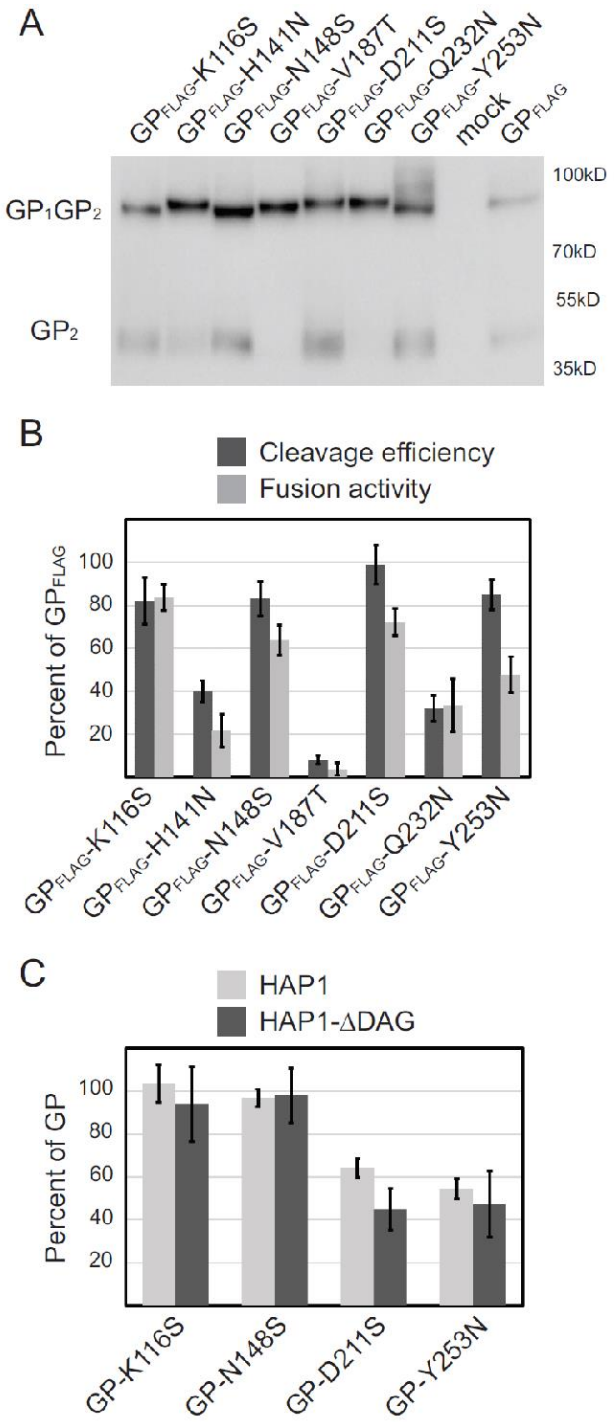

Figure 3.3. Functional analysis of GP1 containing engineered N-linked glycosylation sites. (A) Surface expressed GP of N-glycan mutants and immunoblot analysis using anti-FLAG antibody M2 for detection. (B) Cleavage efficiency and cell-to-cell fusion data. (C) Transduction

of HAP1 and HAP1-ΔDAG1 cells using VSV pseudotyped particles. All data are based on the average and standard error of the mean of at least three replicate experiments.

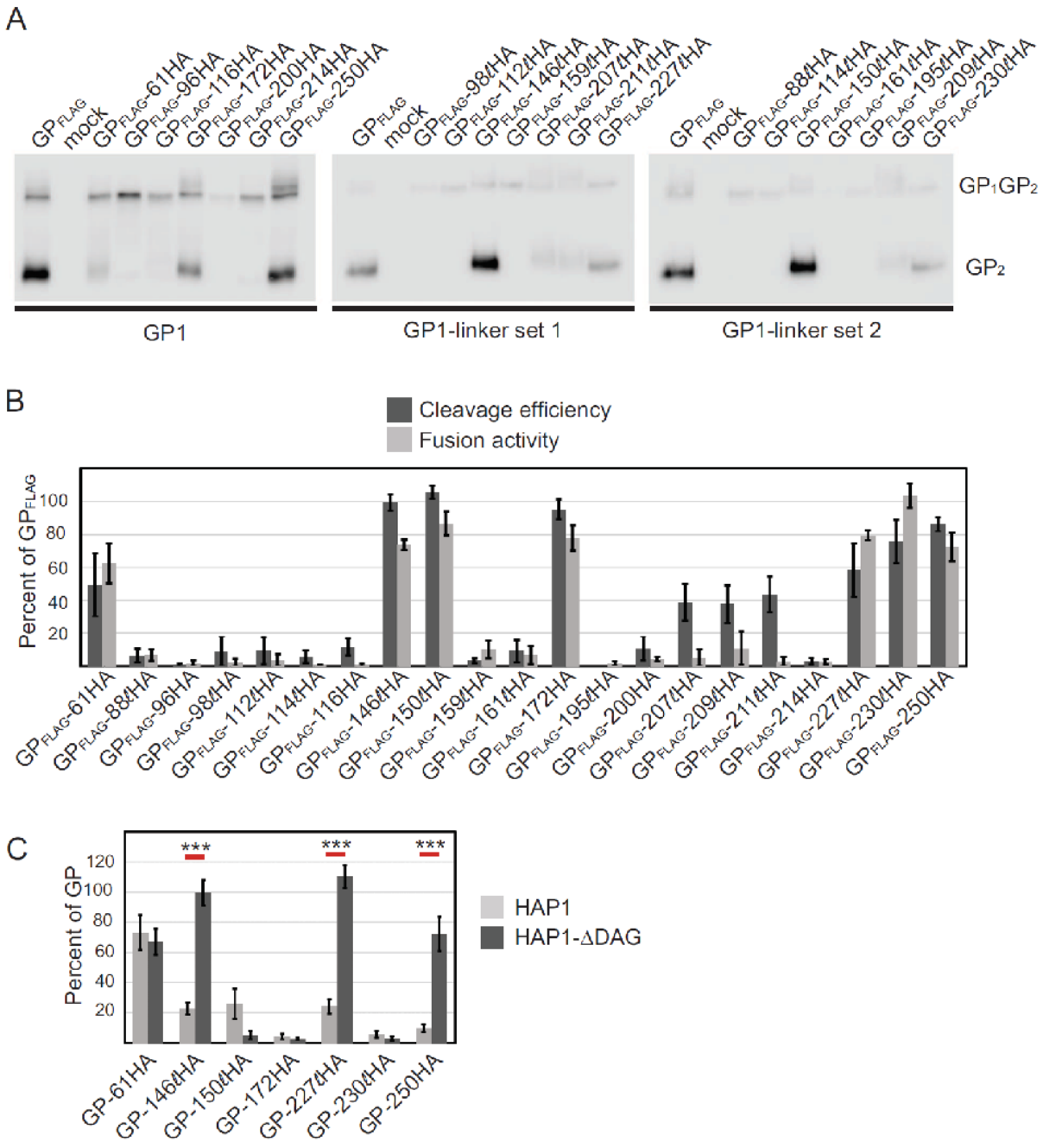

Figure 3.4. Insertional mutagenesis of LASV GPC blocks entry in specific cell lines. (A) Surface expressed HA-tagged mutants and immunoblot analysis detected with anti-FLAG antibody M2. (B) Cleavage efficiency and cell-to-cell fusion data. (C) Transduction of HAP1 and

HAP1-ΔDAG1 cells using VSV pseudotyped particles. All data are based on the average and standard error of the mean of at least three replicate experiments. ***, p-value < 0.001.

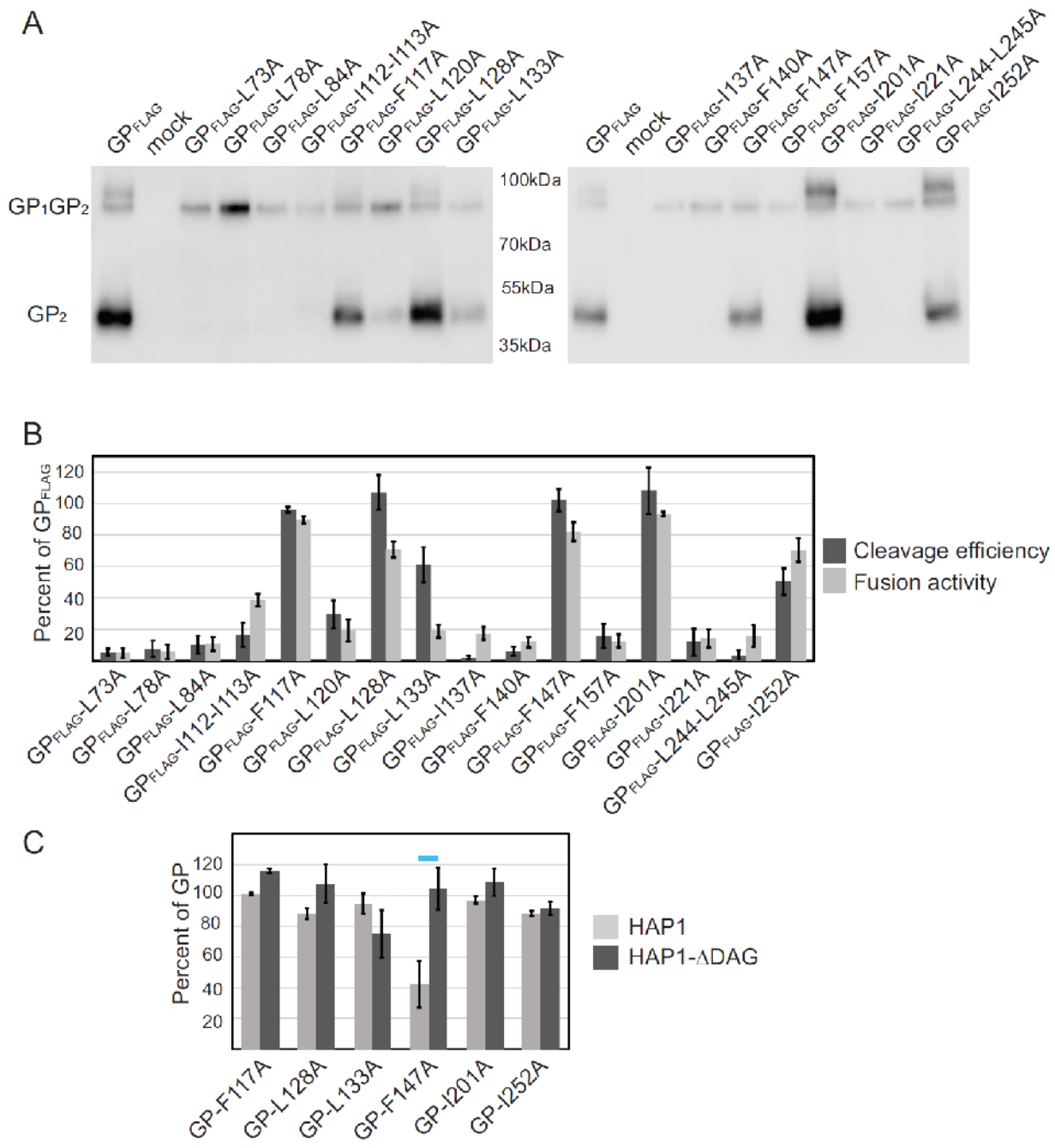

Figure 3.5. Mutating hydrophobic GP1 residues impedes protein processing.

(A) Surface expressed hydrophobic mutants and immunoblot analysis using anti-FLAG antibody M2. (B) Cleavage efficiency and cell-to-cell fusion data. (C) Transduction of HAP1 and HAP1-ΔDAG1 cells using VSV pseudotyped particles. All data are based on the average and standard

error of the mean of at least three replicate experiments. Blue dash highlights the constructs that transduced HAP1-ΔDAG1 similar to parental GP, yet show a defect in HAP1 entry.

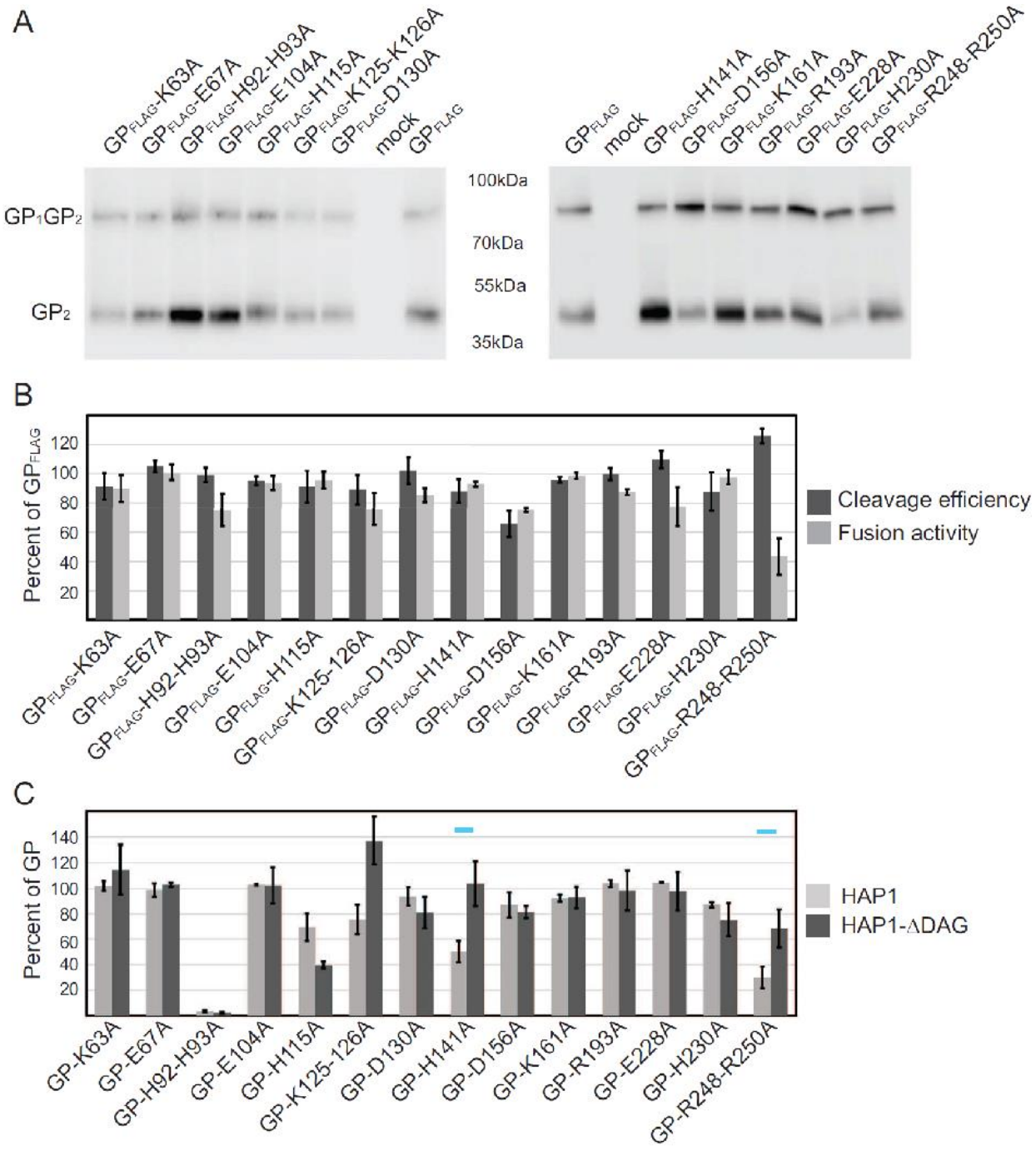

Figure 3.6. Charged GP1 residues are required for efficient HAP1 entry. (A) Surface expressed charged mutants and immunoblot analysis using anti-FLAG antibody M2. (B) Cleavage efficiency and fusion ability data. (C) Transduction of HAP1 and HAP1-ΔDAG1 cells using VSV

pseudotyped particles. All data are based on the average and standard error of the mean of at least three replicate experiments. Blue dash highlights the constructs that transduced HAP1-ΔDAG1 more than twice as efficiently as HAP1 cells.

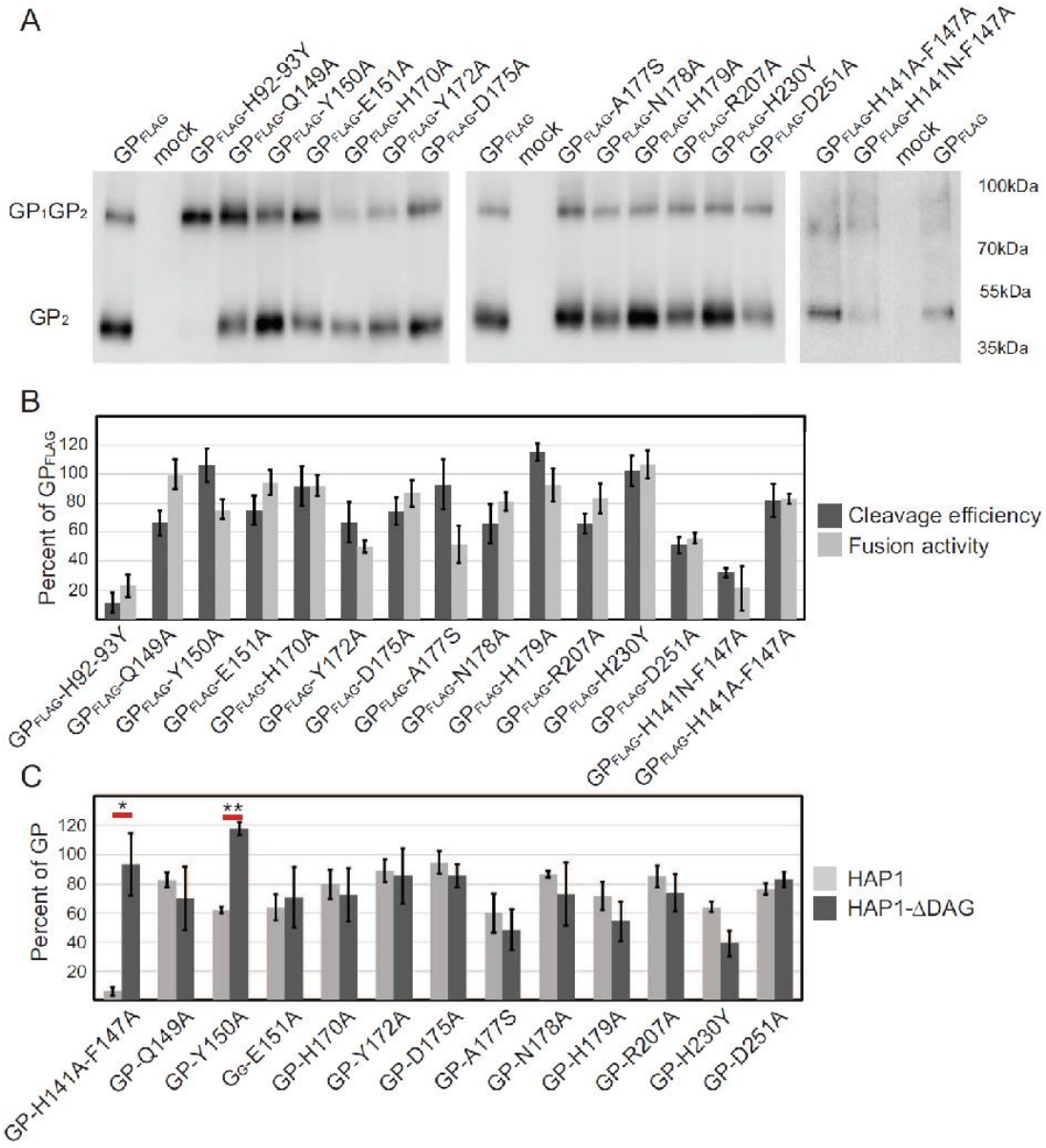

Figure 3.7. Residues involved with the GP1 trimer core are critical for αDG interaction.

(A) Surface expressed targeted GP1 mutants and immunoblot analysis using anti-FLAG antibody M2. (B) Cleavage efficiency and fusion ability data. (C) Transduction of HAP1 and HAP1-ΔDAG1 cells using VSV pseudotyped particles. All data are based on the average and standard error of the mean of at least three replicate experiments. *, p-value <0.05; 88, p-value <0.01.

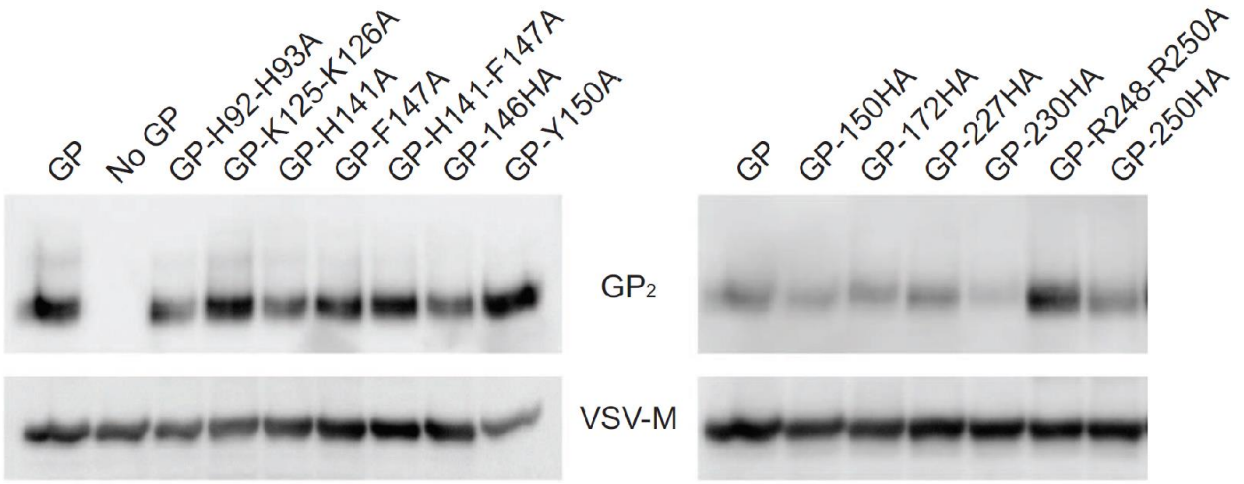

Figure 3.8. GP constructs are efficiently incorporated onto VSV particles. Vero cells were used to produce VSV pseudo-particles. Cell supernatants, containing pseudotyped particles, were collected and precipitated with TCA to determine the level of LASV GP incorporation into VSV envelopes. GP constructs demonstrating low HAP1 transduction, or GP constructs that were unable to transduce both cell types were tested. Precipitated proteins were separated by SDS-PAGE and immunoblotted for LASV GP2 (monoclonal 12.4D) and VSV-M (monoclonal 23H12).

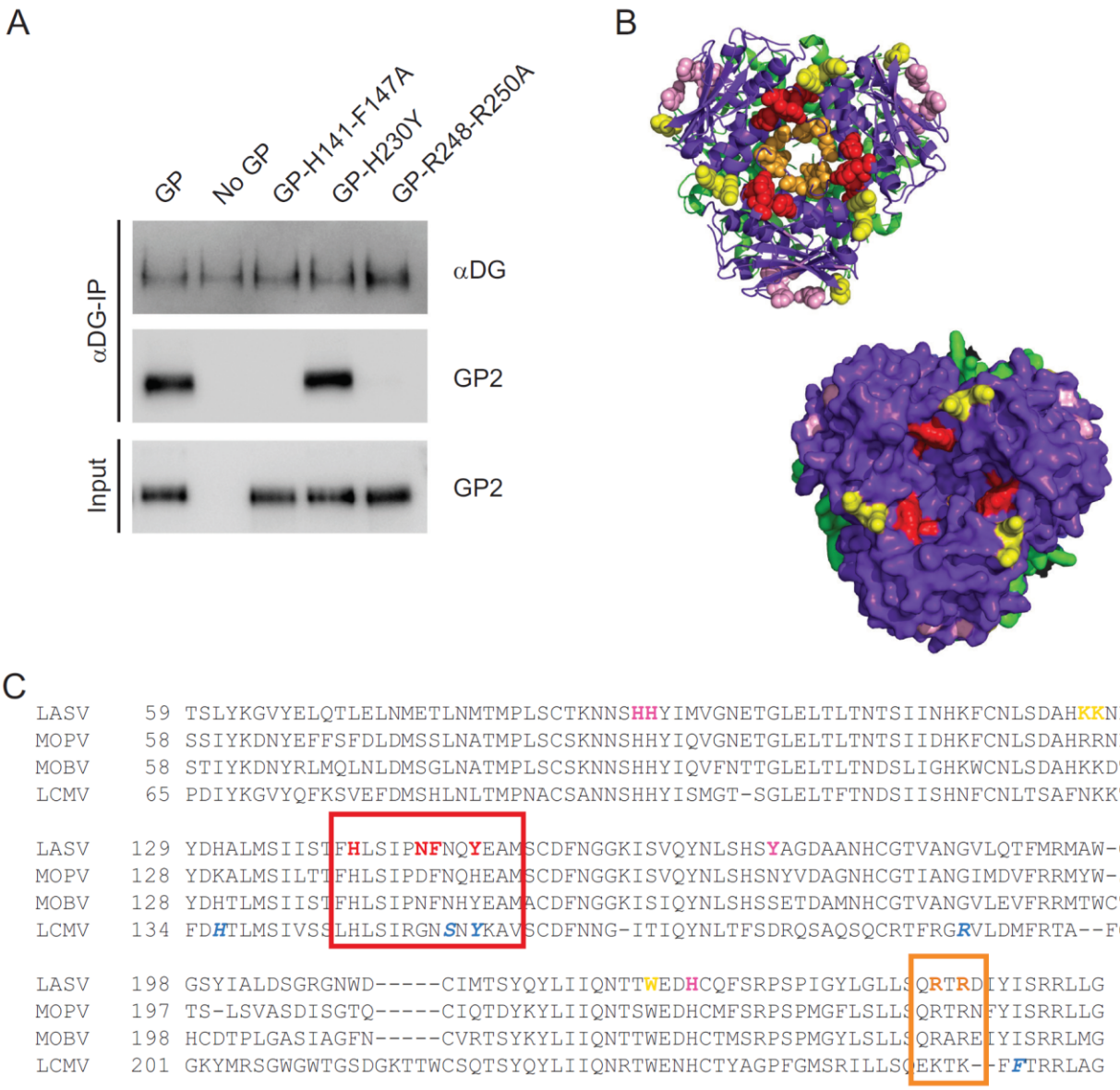

Figure 3.9. Identification and mapping residues implicated in LASV receptor-binding and viral entry. (A) To directly examine GP1 mutant binding, or lack of binding, to αDG, we performed a co-immunoprecipitation assay. αDG coated beads were incubated with VSV

pseudotyped particles containing either parental or mutant LASV GP. All proteins interacting with the αDG coated beads were concentrated and separated by SDS-PAGE. While parental GP and GP-H230Y were able to bind to αDG, GP-H141A-F147A and GP-R248A-R250A were not. (B) LASV GP constructs exhibiting reduced entry into HAP1 cells were mapped onto the LASV pre-fusion crystal structure (PDB 5vk2; GP1 is shown in purple and GP2 is shown in green). Regions that are significantly involved in αDG interactions are shown in red (H141, N146, F147, and Y150). Regions that also demonstrated reduced HAP1 entry are shown in orange (R248 and R250) and yellow (K125, K126 and W227). The histidine triad is shown in pink (H92, H93, and H230). Residues are color coded to match Table 1. Both a cartoon structure and surface rendering of the structure demonstrates that the αDG binding site is located in a cavity on the top of the trimer. (C) Sequence alignment of Old World arenaviruses that use αDG. Regions in LCMV involved in αDG binding are shown in blue, while the regions we have implicated for LASV entry are shown in red. R248 and R250 are highlighted in orange. The histidine triad implicated in LAMP1 interaction are in pink.

Table 3.1. Summary of Fusion, GP cleavage and Transductions

Mutant	Classification	Fusion Activity	Cleavage Efficiency	Transduction Efficiency		Class
				HAP1	HAP1-ΔDAG	
L61HA	HA insertion	62.4 ± 12.1	49.4 ± 19	73.6 ± 11.5	67.9 ± 8.6	III
K63A	Charged	89.8 ± 9.1	91.3 ± 9.3	102.1 ± 3.8	114.5 ± 19.7	III
E67A	Charged	100.8 ± 5.4	104.9 ± 3.8	98.7 ± 5.2	102.9 ± 1.4	III
H92A-H93A	Charged	75.0 ± 10.9	99.1 ± 5.0	3.4 ± 0.8	2.3 ± 0.6	I
T101A	N-gly removal	92.8 ± 0.1	98.9 ± 13.2	96.5 ± 8.7	96.3 ± 17.6	III
E104A	Charged	93.7 ± 4.8	95.5 ± 3.4	102.8 ± 0.5	102.4 ± 14.2	III
S111A	N-gly removal	77.1 ± 6.1	79.4 ± 17.5	101.2 ± 3.9	112.9 ± 12.8	III
H115A	Charged	95.5 ± 5.9	91.3 ± 10.7	69.6 ± 10.9	39.9 ± 2.7	III
K116S	N-gly addition	83.6 ± 6.0	82.1 ± 11.5	103.5 ± 6.6	93.9 ± 8.8	III
F117A	Hydrophobic	89.4 ± 2.2	96.3 ± 1.8	101.1 ± 0.6	116.1 ± 1.7	III
S121A	N-gly removal	64.0 ± 5.5	86.8 ± 12.5	98.6 ± 4.4	121.0 ± 9.8	III
K125A-K126A	Charged	76.0 ± 10.6	89.5 ± 10.2	75.6 ± 11.4	137.2 ± 18.4	II
L128A	Hydrophobic	70.8 ± 5.0	107.0 ± 11.1	88.3 ± 3.5	107.8 ± 12.4	III
D130A	Charged	85.0 ± 4.8	102.3 ± 9.0	93.7 ± 7.3	81.0 ± 12.4	III
L133A	Hydrophobic	19.0 ± 4.2	61.0 ± 11.2	94.7 ± 6.7	75.0 ± 15.6	III
H141A	Charged	92.7 ± 1.7	87.8 ± 8.3	50.3 ± 8.7	103.7 ± 17.5	II
F147A	Hydrophobic	82.0 ± 5.9	102.1 ± 7.0	42.2 ± 15.1	104.5 ± 13.7	II
H141A-F147A	Targeted	82.8 ± 3.3	81.6 ± 11.4	17.4 ± 2.8	93.5 ± 21.5	II
N146lHA	HA + linker	73.7 ± 3.1	99.4 ± 4.8	23.0 ± 3.8	100.5 ± 11.7	II
N148S	N-gly addition	63.8 ± 7.1	83.3 ± 7.9	96.7 ± 4.9	97.9 ± 11.0	III
Q149A	Targeted	99.6 ± 10.2	66.5 ± 8.5	83.1 ± 4.9	70.1 ± 21.8	III
Y150A	Targeted	75.5 ± 6.7	105.9 ± 11.6	62.2 ± 2.3	117.9 ± 4.4	II
Y150lHA	HA + linker	86.6 ± 7.2	105.8 ± 3.9	26.0 ± 10.1	5 ± 0.8	I
E151A	Targeted	94.1 ± 8.7	75.1 ± 10.1	64.1 ± 9.0	70.9 ± 20.8	III
D156A	Charged	75.4 ± 1.4	66.1 ± 8.5	87.0 ± 9.8	81.4 ± 4.6	III
K161A	Charged	98.6 ± 2.1	96.1 ± 1.8	92.2 ± 2.6	93.0 ± 8.6	III
S169A	N-gly removal	63.7 ± 9.9	58.4 ± 18.4	87.6 ± 4.7	112.8 ± 15.3	III
H170A	Targeted	91.2 ± 7.5	91.5 ± 13.8	80.0 ± 10.0	72.7 ± 18.2	III
Y172A	Targeted	50.0 ± 4.3	66.6 ± 13.8	89.3 ± 7.9	85.5 ± 19.0	III
Y172HA	HA insertion	77.9 ± 7.6	95.4 ± 5.9	4.3 ± 1.8	4.6 ± 2.5	I
D175A	Targeted	86.6 ± 9.1	74.4 ± 9.5	95.1 ± 7.9	85.6 ± 8.0	III
A177S	Targeted	51.4 ± 12.8	92.7 ± 17.2	60.1 ± 13.4	48.6 ± 14.3	III
N178A	Targeted	81.1 ± 6.1	65.9 ± 13.3	86.9 ± 2.4	73.2 ± 21.8	III
H179A	Targeted	92.6 ± 11.4	115.3 ± 6.1	71.9 ± 9.8	54.5 ± 13.3	III
R193A	Charged	87.5 ± 1.9	99.7 ± 3.7	103.9 ± 2.9	98.5 ± 15.6	III
I201A	Hydrophobic	93.3 ± 1.6	108.0 ± 14.8	97.1 ± 2.3	108.8 ± 8.9	III
R207A	Targeted	83.4 ± 10.2	65.8 ± 6.7	85.4 ± 7.2	74.2 ± 12.9	III
D211S	N-gly addition	72.3 ± 6.3	99.5 ± 8.9	64.1 ± 18.5	44.7 ± 9.7	III
T226A	N-gly removal	58.6 ± 7.5	82.4 ± 20.7	75.3 ± 10.6	85.9 ± 6.6	III
W227lHA	HA + linker	79.5 ± 2.9	58.5 ± 16	24.3 ± 4.8	103.7 ± 4.1	II

E228A	Charged	77.7 ± 13.4	109.7 ± 5.8	104.6 ± 0.3	97.8 ± 15.0	III
H230A	Charged	97.7 ± 4.8	87.6 ± 13.5	87.3 ± 2.1	75.4 ± 13.0	III
H230Y	Targeted	106.7 ± 9.7	102.3 ± 10.3	64.1 ± 3.5	39.4 ± 3.9	III
H230lHA	HA + linker	103.8 ± 7.3	75.8 ± 13	5.9 ± 2.2	5.3 ± 3.1	I
R250HA	HA insertion	72.3 ± 8.6	86.2 ± 4	10.2 ± 2.6	82.5 ± 7	II
D251A	Targeted	55.7±3.9	50.9 ± 5.4	76.6 ± 3.9	83.2 ± 5.2	III
R248A-R250A	Charged	43.4 ± 12.3	128.9 ± 4.9	30.2 ± 8.5	68.5 ± 15.0	II
I252A	Hydrophobic	70.5 ± 7.5	50.5 ± 8.3	88.3 ± 1.6	91.8 ± 4.3	III
Y253N	N-gly addition	47.7 ± 8.3	84.9 ± 7.2	54.4 ± 15.0	47.2 ± 10.9	III

I: Transduction reduced in both cell types; II: Transduction reduced in HAP1 cells compared to HAP1-ΔDAG cells; III: No receptor binding defects

Chapter 4

MUTATIONAL ANALYSIS OF LASSA VIRUS GP2 SUBUNIT HIGHLIGHTS REGIONS REQUIRED FOR PROTEIN FUNCTION

Introduction and Objectives

Arenaviruses are endemic to many countries throughout the world and are divided into two subgroups based on geographic distribution: Old World and New World arenaviruses. Both subgroups contain human pathogens capable of causing severe hemorrhagic fever with high morbidity and mortality. Lassa virus (LASV) is an Old World arenavirus endemic to West Africa and the agent that causes Lassa Fever. Each year several hundred-thousand people become infected with LASV and those infections result in nearly 5,000 deaths (85). Human infections occur from zoonotic spread from a rodent host. The main rodent host for LASV is *mastomys natalensis*; in 2016 two other potential reservoirs were found *Hylomyscus pamfi* and *Mastomys erythroleucus* (12, 13). Lassa virus infection can occur through many routes including aerosolization of contaminated rodent excrement, abrasions on skin, and infectious body fluids (10). Due to the lack of vaccines and effective therapeutics, LASV is categorized as a class A pathogen (86).

The arenavirus particle consists of a host derived lipid envelope and contains a bi-segmented RNA genome in ambisense orientation. Embedded in the envelope are mature trimeric viral glycoprotein (GP) spikes which are necessary for attachment and entry. The glycoprotein precursor (GPC) is produced in infected cells as a type I membrane protein which is then processed twice by host cell peptidases. The first processing event occurs in the ER by a cellular peptidase, producing the stable signal peptide (SSP) subunit. The second processing event occurs in the cis-Golgi by subtilisin kexin isozyme-1/site-1 protease (SKI-1/S1P) which produces the GP1 and GP2

subunits (44, 46, 87). Unlike traditional class I fusion proteins, the SSP of arenaviruses is not degraded but becomes part of the trimeric glycoprotein complex. The SSP assists in many chaperone roles including protein processing, trafficking, and pH sensing (48, 49, 88). While the function of GP1 and GP2 is to mediate receptor interactions and membrane fusion respectfully (53-55, 58, 89).

To overcome lipid membrane boundaries, enveloped viruses encode proteins capable of mediating fusion between the viral and cellular membranes. The fusion event for LASV GP occurs in an endo-lysosomal compartment under low-pH (52). Presumably, interaction between GP1 and lysosomal associated membrane protein 1, LAMP1, lowers the energy barrier needed for fusion protein activation (64). Triggering of GP2 drives the merger of viral and host cell membranes to create a fusion pore that the viral genome is shuttled through.

The pre-fusion LASV GP2 and post-fusion lymphocytic choriomeningitis virus (LCMV) GP2 have been crystalized (50, 54). Due to the high sequence similarity between OW arenaviral GP2 proteins, we can utilize the low-pH crystal of LCMV to infer the structure of post-fusion LASV GP2. The arenavirus fusion protein encodes two heptad repeat (HR) domains, a single pass transmembrane domain and a fusion peptide (N-FP) similar to retroviruses, filoviruses, paramyxoviruses, and influenza (53). Unlike typical class I fusion proteins, the arenavirus GP2 also encodes for an internal fusion loop (I-FP). Under low-pH, the arenaviral GP undergoes major conformational changes to mediate viral fusion. First, the fusion peptide/loop is inserted into the host membrane. After multiple GP2 subunits are triggered, and the energy requirements to overcome membrane barriers are met, the glycoproteins collapse in an energetically favorable conformation known as a six-helix bundle (6HB) (Fig 4.1). Formation of 6HB is mediated by HR1

and HR2 rearrangements transitioning from the hairpin conformation to 6HB. Full collapse of the glycoprotein allows for fusion pore formation and genome release into the cytoplasm (65).

In an attempt to better understand residues involved GP2 function, we utilized alanine scanning mutagenesis to identify conserved residues critical in the fusion process. We hypothesized that charged and hydrophobic residues residing in or near the previously defined GP2 functional domains are required for GP2 mediated fusion. Through biochemical analysis, we identified several charged and hydrophobic residues that inhibit functions of the LASV GP2 subunit. Mutations which caused impaired GP2 function were located in or near HR1, HR2, the fusion peptide or fusion loop. Each of these domains are required and function together to facilitate the glycoprotein mediated fusion event.

Materials and Methods

Cell lines and transfections. Vero (African green monkey kidney) cells stably expressing human SLAM were maintained in Dulbecco's modified Eagle's medium (DMEM) supplemented with 5% (vol/vol) fetal bovine serum (FBS) and kept at at 37°C and 5% CO_2 (90). HAP1 and HAP1-ΔDAG1 cells (Horizon) were maintained in Iscove's media supplemented with 10% (vol/vol) FBS and kept at 37°C and 5% CO_2. All transient transfections were performed using GeneJuice (Millipore) according to the manufacturer's instructions.

Molecular biology. The LASV GPC protein coding sequence was codon optimized for mammalian expression and cloned into a pcDNA3.1intron vector. Gene expression was initiated by a CMV promotor and the β-globin intron was engineered in the 5' untranslated region (UTR) to increase protein production. A carboxy-terminal 3xFLAG tag was added to the cytoplasmic tail of the GP2 subunit for biochemical detection of charged constructs. Point mutations were

introduced with QuikChange mutagenesis and PfuTurbo-HS polymerase (Agilent). Sequence analysis for each plasmid DNA was carried out, and the presence of the mutation was confirmed. Complete sequence information is available upon request.

Surface biotinylation. Vero cells were transfected with plasmid DNA encoding the indicated Lassa GPC construct. Thirty-six hours following transfection, cells were washed with cold PBS and biotinylated with 0.5 mg/mL sulfosuccinimidyl-2-(biotinamido) ethyl-1,3-dithiopropionate (Thermo) for 30 min on ice. The reaction was quenched using Tris-HCl, and cells were lysed in M2 lysis buffer (50 mM Tris, pH 7.4, 150 mM NaCl, 1 mM EDTA, 1% Triton X-100) at 4°C and clarified with centrifugation (20,000xg, 15 min). Lysate was incubated with streptavidin sepharose beads (GE Healthcare) for 60 min while rotating. Following incubation, the streptavidin sepharose beads were washed in buffer 1 (100 mM Tris (91), 500 mM lithium chloride, 0.1% Triton X-100) and then in buffer 2 (20 mM HEPES [pH 7.2], 2 mM EGTA, 10 mM magnesium chloride, 0.1% Triton X-100), incubated in urea buffer (200 mM Tris, pH 6.8, 8 M urea, 5% sodium dodecyl sulfate [SDS], 0.1 mM EDTA, 0.03% bromophenol blue, 1.5% dithiothreitol) for 30 min at 55°C, and subjected to immunoblot analysis.

Antibodies and immunoblots. Surface biotinylated material was fractionated by gel electrophoresis on 10% Tris-glycine gels (ThermoFisher) and transferred to polyvinylidene difluoride (PVDF) membranes (GE Healthcare). GP was detected with specific antibodies directed against the Flag epitope tag (M2; Sigma) or against LASV GP2 (22.5D), kindly provided by Dr. James Robinson (Tulane University). Immunoblots were developed using mouse IgG horseradish peroxidase (HRP)-conjugated secondary antibodies (Jackson) and a ChemiDoc digital imaging system (Bio-Rad). Immunoblots were quantified using ImageLab software.

Cell-to-cell fusion assay. Vero cells were co-transfected with Lassa GP mutants and pmaxGFP (4:1 ratio). Forty hours following transfection, media was removed and replaced with DPBS (pH 4) and incubated (37°C and 5% CO_2) for 30 min to allow glycoprotein triggering. The DPBS was replaced with DMEM and cells were incubated for an additional 3 hours to enable membrane rearrangement and syncytia formation. Four representative pictures of the fusion were taken using Zoe microscope (Bio-Rad) (20x magnification) and unfused cells were counted. Quantification of fusion was calculated using the following equation:

$$Fusion = \frac{(unfused\ cells\ in\ mock\ transfected - unfused\ cells\ in\ mutant\ transfected)}{(unfused\ cells\ in\ mock\ transfected - unfused\ cells\ in\ WT\ GPC\ transfected)} \times 100$$

Each mutant was assessed in the fusion assay in three independent experiments.

VSV pseudotype production and transductions. GP constructs lacking the c-terminal 3xFlag tag were used to make the vesicular stomatitis virus (VSV) pseudotyped particles. Vero cells were transfected with LASV GP DNA. Thirty-six hours following transfection the cells were transduced with VSVΔG-GFP particles pseudotyped with VSV-G (MOI 1) for one hour (courtesy of Dr. Michael Whitt; KeraFAST) (94). The particle-containing media was then replaced with fresh DMEM. VSVΔG-GFP particles displaying the LASV GP were collected 12 hours following the transduction. These particles were applied onto HAP1 and HAP1-ΔDAG1 cells in volumes of 0.25 mL and 1 mL, respectively. A higher volume of particles was used to transduce HAP1- ΔDAG1 cells in order to overcome the decreased transduction efficiency when the cells are missing the primary receptor (58). The number of GFP positive cells was enumerated in a flow cytometer. Results are displayed as the percent of GFP positive cells present in a population of 10,000 live cell events compared to GP wild-type transduction.

Results

Characterization of Charged Constructs

Charged amino acid residues play critical roles in protein organization and function (115). Previous studies of the arenaviral GP2 subunit have characterized the C- terminal domain required for SSP interactions and several hydrophobic amino acids within the fusion peptide and fusion loop (88, 107). However, there has not been an extensive characterization of the GP2 subunit as a whole. We mutated and characterized 31 conserved charged residues throughout the fusion active subunit of LASV. The 31 constructs were expressed in Vero cells, those present on the surface were biotinylated, concentrated with streptavidin beads and analyzed through western blot to determine the constructs expression and cleavage efficiencies (Fig 4.2A)., with the exception of E308A and H467A-R468A, all mutant constructs were processed to some degree, evidenced by the GP2 bands (Fig 4.2A).

To determine if the charged constructs produced functional GP, we assessed fusion activity using a cell-to-cell based fusion assay. Incubating cells expressing LASV GP with a low-pH buffer mimics the low-pH environment in the lysosome and results in robust syncytia formation. Fusion efficiency is determined by comparing the extent of syncytia formation caused by the mutant and parental GP. Several constructs, in or near functional domains, expressing processed GP2 (D268A, R282A, K291A, K471A and R422A) caused a reduction (<25%) in fusion compared to wild-type LASV GP. Other mutated residues within these domains, which did not affect fusion, may be more tolerant of mutations (Fig 4.2B).

Our cell-to-cell fusion assay bypasses virus entry and only tests for the ability of GP2 to trigger at an artificially low-pH. To test if the GP2 mutations affect viral entry, we utilized a VSV

pseudotyping system to incorporate our GP constructs onto a VSV particle lacking its native glycoprotein. VSV-LASV GP particles require LASV receptor usage for entry and trafficking to an endo-lysosomal compartment for efficient GP triggering. A factor that could cause differences seen between our cell-to-cell fusion assay and transduction assay is the pH which the GP is exposed to. The pH in a lysosomal compartment ranges from 4.5 to 5 which is higher than the pH 4 buffer used in our cell-to-cell fusion assay (116). Mutations that alter pH sensitivity may allow for syncytia formation in our cell-to-cell fusion assay and alter transduction efficiency. The two haploid cell lines used in our transduction assay have been extensively characterized for LASV entry (58, 59). Both are used here for the efficient characterization of our GP constructs.

Glycoprotein processing is required for fusion; therefore, we only examined transduction efficiency for constructs expressing >20% cleaved GP2, and >40% fusion/cleavage efficiency compared to wtLASV GP. Because we only tested fusion competent constructs in our transduction assay we expected all constructs to efficiently enter the haploid cell lines tested. In total, 20 constructs were assayed for their ability to transduce HAP and HAP-ΔDAG cell lines. Because GP2 is not thought to directly be involved in receptor interactions, little difference was expected between cell line transduction efficiencies. All constructs were able to effectively gain entry into the HAP1 cell lines tested except for one construct (K465A) which did not efficiently transduce into either HAP cell line (Fig 4.2C).

Characterization of Hydrophobic Residues

Hydrophobic residues within viral fusion proteins are involved in protein folding and many functional domain processes. Previous studies have identified hydrophobic residues within the fusion domains and C-terminus of the arenaviral GP2 subunit that are required for fusion (107).

We expanded the number of GP2 mutations and characterized 29 constructs. Mutations were made throughout the GP2 subunit to identify conserved residues involved in GP structure and function. Cell surface expression of the glycoprotein constructs and processing was analyzed through surface biotinylation. A majority of the constructs were cleaved but there were several constructs (F293A, F309A, L315A-F316A, L344A-I345A and L372A) that did not produce detectible GP2 with immunoblot analysis (Fig 4.3A). Three of our hydrophobic constructs had been previously characterized; however, our cleavage data for two constructs differed. Surface biotinylation data carried out by Klewitz et al. showed that F262A and L266A were unable to become surface expressed, but underwent some processing as seen in their total lysate blot (107). Our data disputes their data and suggests that both F262A and L266A are surface expressed near wtGP levels (Fig 4.3A). The difference in these phenotypes could be because we allow our transduction to incubate for 36 hours versus 24 hours.

To determine if the hydrophobic constructs produced functional protein, we again assessed the constructs in our cell to-cell fusion assay. Many of the hydrophobic mutations resulted in reduced or completely abolished cell-to-cell fusion. In total, there were eight processed hydrophobic constructs that fused <25% compared to wild-type LASV GP (Fig 4.3B). Of the eight constructs, five were located within GP2 functional domains including the internal fusion peptide and HR1/HR2 domains. The three constructs (394A, 399A and 415A) that negatively impacted fusion and were not located within functional domains were positioned near the HR1 and HR2 domains (Fig 4.3B).

Transduction was carried out for ten constructs that expressed over 20% surface expressed GP2, and above 40% cleavage and fusion efficiency (Fig 4.3C). Again, transduction into HAP and

HAP-ΔDAG cell lines followed a similar trend. There were three constructs (313A, 361A and 387A) that expressed transduction phenotypes which were less than half off their fusion activity. The other seven constructs expressed similar transduction ability and fusion activity (Fig 4.3C).

Discussion

Here we produced and characterized a library of 60 constructs to provide the groundwork for identifying residues involved in GP2 function and fusion mechanisms. Of our 60 constructs, 29 mutations were located within GP2 functional domains. Each construct was tested for protein processing, expression and fusion. Transduction was carried out with constructs expressing over 20% surface expressed cleaved GP2 and over 40% processing and fusion. Previously defined haploid cell lines were used to carry out viral transduction to assess the differences between our cell-to-cell fusion assay and an intact viral pathway (58, 59). These data highlight residues involved in mediating cell fusion and allowing particle entry. Constructs that were expressed and processed but were unable to mediate efficient cell-to-cell fusion at low-pH will be tested in future biochemical assays to determine where in the entry pathway the mutation is affecting.

In total, 5 of the produced charged constructs expressed fusion defects below 25 percent, and only two of the fusion defective constructs were located in a functional domain. Both basic residues (R282 and K291) within the I-FP caused fusion defects when mutated. Residue R282 is positioned adjacent to E289 and under low-pH these residues may play structural roles to properly position the fusion loop and mediate membrane merger (50). Under neutral pH, residue K291 is in close proximity to the N-terminus of GP1 (50). If interactions between K291 and T70 within GP1 occur, it may help to position the fusion loop for when GP1 conformational changes occur. Other charged residues which cause fusion deficiencies when mutated include D268, K417 and R422.

Although these residues fall outside of the GP2 functional domains they seem to be important for mediating virus induced fusion. We can speculate on how residue D268 may be involved in the fusion process due to its incorporation in a recently published LASV GP crystal structure (50). The aspartic acid residue at position 268 is located between the N-FP and I-FP and in close proximity to K272. This charge-charge interaction may help structure the region around the fusion peptide and fusion loop required for mediating membrane merger. Residues K417 and R422 are not incorporated in either the neutral or low-pH GP2 crystal structures but are located between HR2 and transmembrane domain (50, 54). These residues could also play key roles in GP2 structural rearrangements leading to membrane merger.

Eight of the produced hydrophobic constructs resulted in fusion defects below 25 percent. Two mutations (L280A and L285A-I286A) within I-FP resulted in impaired fusion which suggests that these residues may be critical for I-FP insertion. It was expected that altering hydrophobic residues within this domain would cause fusion defects because hydrophobic residues within viral fusion peptides/fusion loops are required to insert into the host membrane. One residue, I323, located in the HR1 domain and two other residues, I403 and I411, located in the HR2 domain also resulted in fusion defects when mutated. Residue I323 is located in the region of HRI that interacts with HR2 to form 6HB, so it is possible that the I323A mutation may impair fusion by interrupting 6HB formation (54). Residues I403 and I411 located within HR2 may also be involved in 6HB formation and mediating viral-host membrane merger (54). Therefore, mutations to these residues could impair GP mediated fusion by blocking 6HB formation. Other residues which negatively impacted fusion but were not located in GP2 functional domains include L394, F399 and L415A. In the post-fusion GP2 state, L394 and F399 are located within an unstructured loop which

interacts with HR1 and interruption of these interactions could inhibit fusion pore formation (54). L415 is the residue directly after the HR2 domain and interruption of this residue presumably inhibits 6HB formation (54).

Viral transduction was carried out for constructs expressing over 20% surface expressed GP2, and over 40% fusion and cleavage efficiency. While all constructs were able to transduce at some level, a subset of constructs (R356A, I361A, L387A and K465A) expressing near wtGP levels of cell-to-cell fusion were unable to mediate high transduction levels. These mutations may cause GP2 to become less sensitive to low-pH and the endo-lysosomal pH is not low enough to allow for efficient GP triggering.

Taken together, these data demonstrate that both conserved hydrophobic and charged residues throughout GP2 are required for protein function. Specifically, residues near or within the I-FP, HR1 and HR2 domains play critical roles within the fusion process. Residues involved in the structure or insertion of I-FP include L280, L285-I286, R282 and K291. Residues which may be involved in 6HB formation include I323, R355, L394, F399, I404, I411 and L415. There were also several amino acids (D268, K368, K417, R422 and K461) outside of defined structural domains that negatively affected fusion. Further experiments will be required to biochemically test where in the fusion process these mutations are affecting.

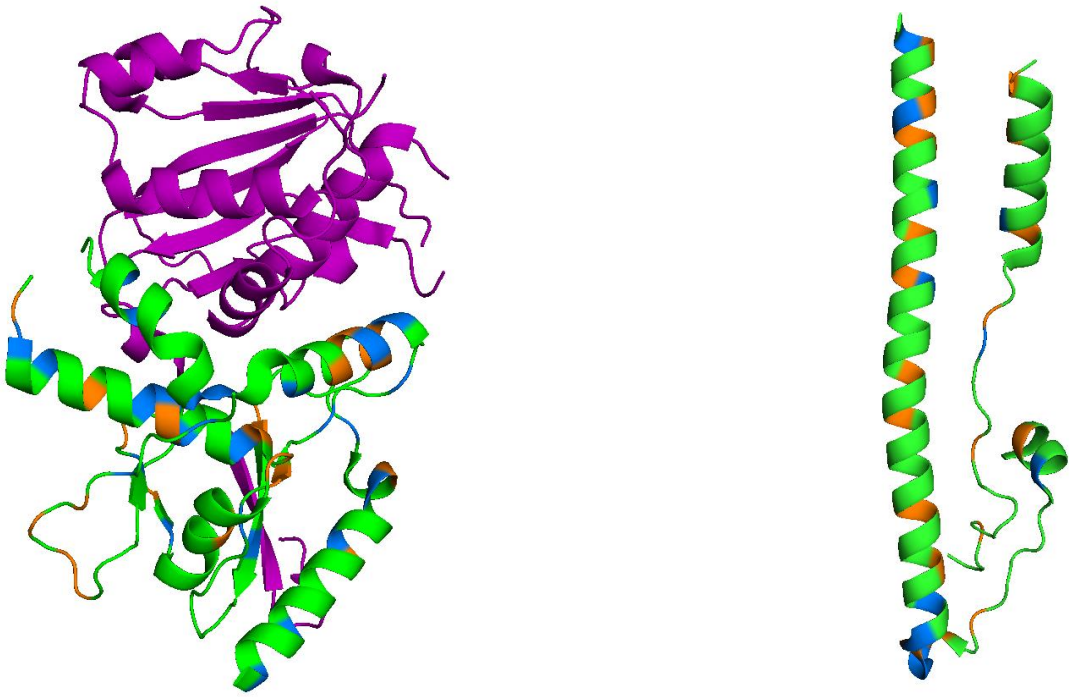

Figure 4.1. Mapping the charged and hydrophobic mutations on LASV GP2 pre- and post-fusion states. (left) The LASV GP1-GP2 pre-fusion crystal structure (PDB 5vk2), rotated 180° (50). The GP1 subunit is shown in purple and the GP2 subunit is shown in green. (right) The LASV GP2 post-fusion GP2 crystal structure (3mko) (54). Mutations produced throughout the GP2 subunit are color-coded as follows: charged-alanine (blue) and hydrophobic-alanine (orange). Mutated residues which were not located in crystalized regions are not represented in the structures above. All structures were rendered with PyMol.

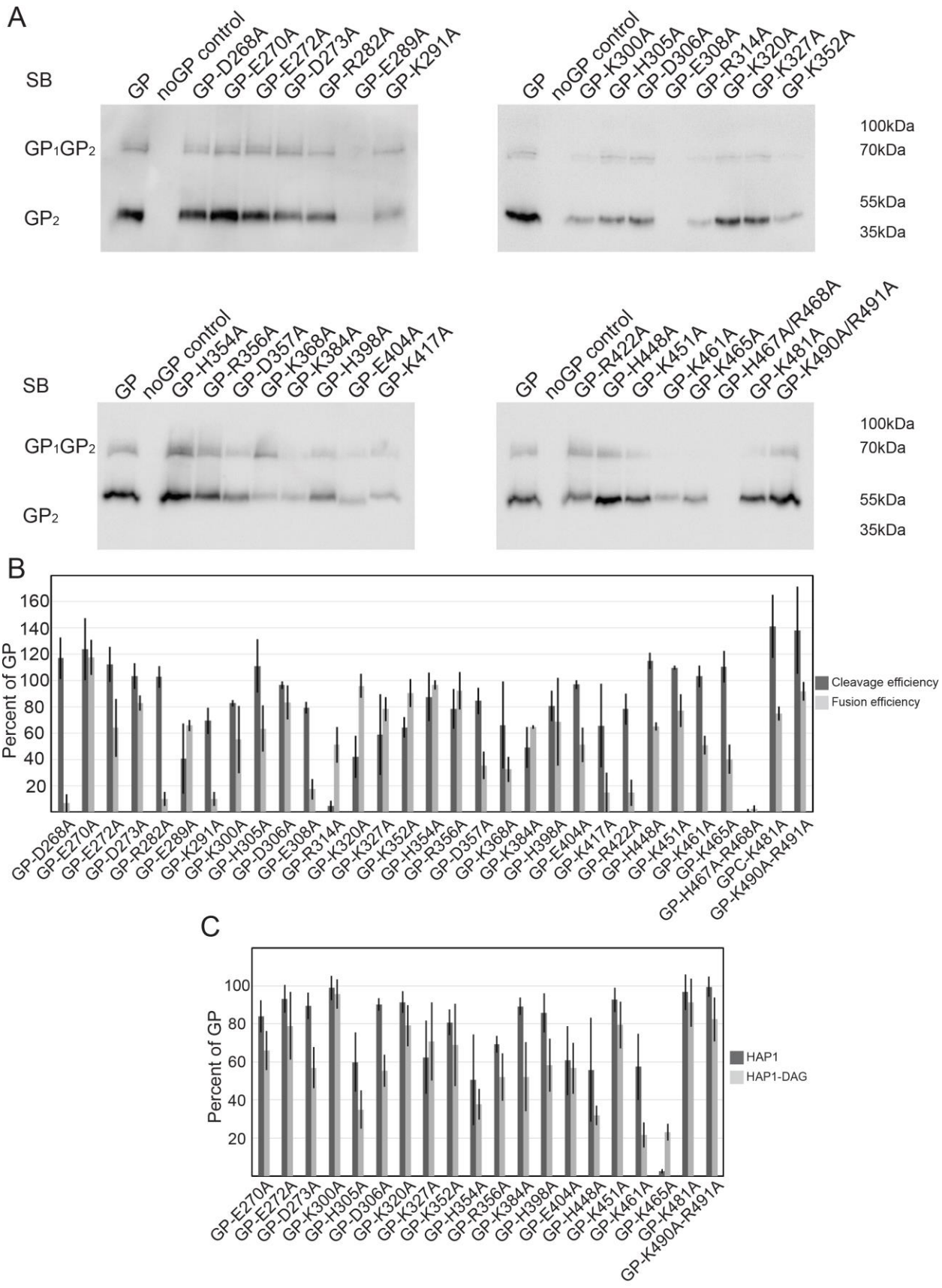
A
SB
GP
noGP control
GP-D268A
GP-E270A
GP-E272A
GP-D273A
GP-R282A
GP-E289A
GP-K291A
GP-K300A
GP-H305A
GP-D306A
GP-E308A
GP-R314A
GP-K320A
GP-K327A
GP-K352A
GP-H354A
GP-R356A
GP-D357A
GP-K368A
GP-K384A
GP-H398A
GP-E404A
GP-K417A
GP-R422A
GP-H448A
GP-K451A
GP-K461A
GP-K465A
GP-H467A/R468A
GP-K481A
GP-K490A/R491A
GP1GP2
GP2
100kDa
70kDa
55kDa
35kDa
B
Percent of GP
Cleavage efficiency
Fusion efficiency
C
Percent of GP
HAP1
HAP1-DAG

Figure 4.2. Processing and functional characteristics of conserved charged GP2 residues. (A) Vero cells transduced with the indicated LASV GP constructs were subjected to cell surface biotinylation after 36 hours. Biotinylated proteins were concentrated using streptavidin sepharose beads, denatured and separated by SDS-PAGE. LASV GP was detected using an anti-FLAG antibody, M2, against the C-terminal GP2 3x flag tag. (B) Cleavage efficiency and cell-to-cell fusion data was quantified as previously stated. (C) VSVΔG-LASV GP constructs encoding GFP were used to transduce HAP1 and HAP1-ΔDAG1 cells; efficiently transduced cells expressed GFP. Transduction was quantified using flow cytometry gating for GFP positive cells. Transduction efficiency, for each construct, was normalized to wild-type LASV GP particle transduction for both cell lines tested. All data are based on the average and standard error of the mean of at least three replicate experiments.

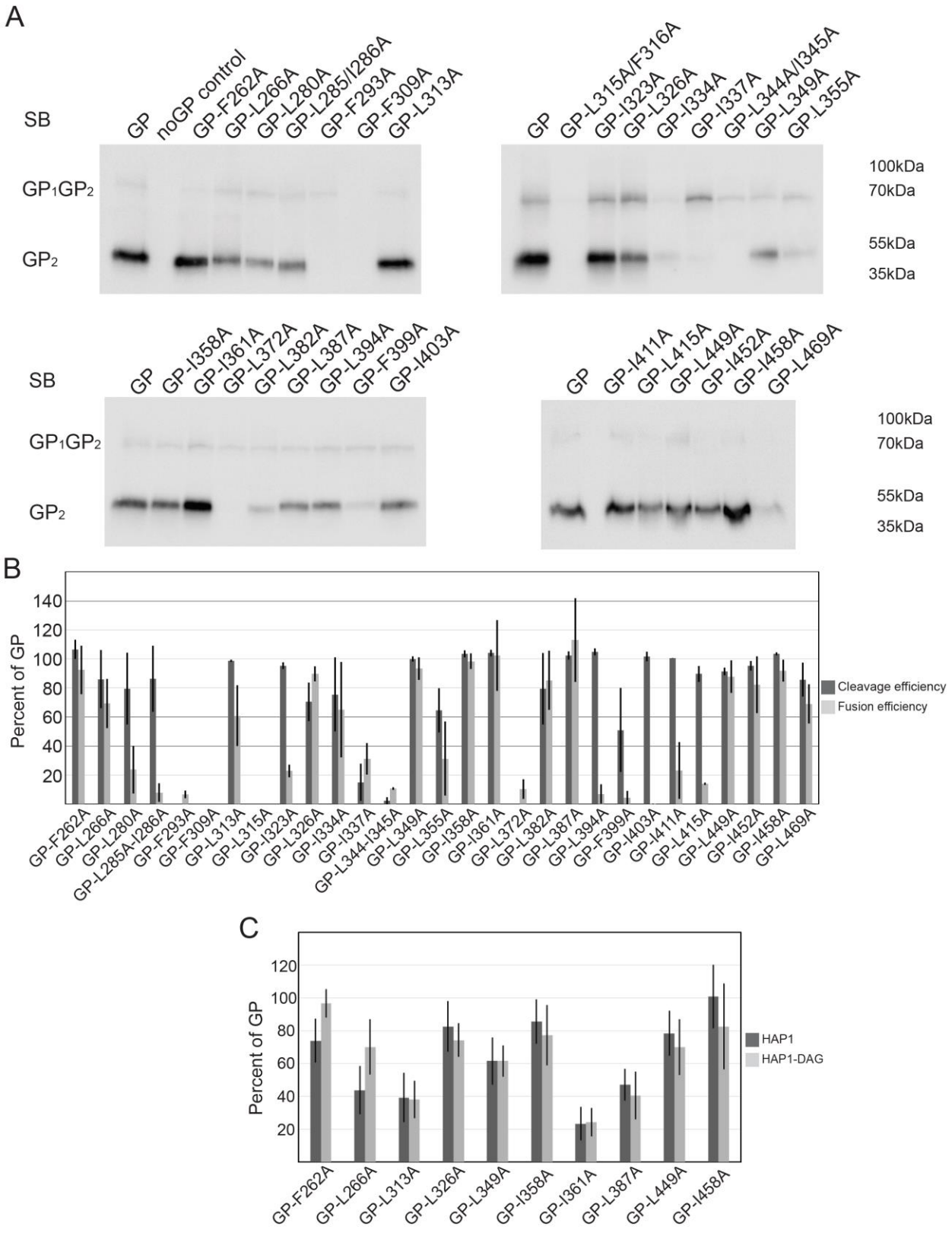
A
SB
GP
noGP control
GP-F262A
GP-L266A
GP-L280A
GP-L285/I286A
GP-F293A
GP-F309A
GP-L313A
GP-L315A/F316A
GP-I323A
GP-L326A
GP-I334A
GP-I337A
GP-L344A/I345A
GP-L349A
GP-L355A
GP1GP2
GP2
100kDa
70kDa
55kDa
35kDa
GP-I358A
GP-I361A
GP-L372A
GP-L382A
GP-L387A
GP-L394A
GP-F399A
GP-I403A
GP-I411A
GP-L415A
GP-L449A
GP-I452A
GP-I458A
GP-L469A
B
Percent of GP
Cleavage efficiency
Fusion efficiency
C
HAP1
HAP1-DAG

Figure 4.3. Processing and functional characteristics of conserved hydrophobic GP2 residues. (A) Surface expressed hydrophobic constructs were examined through SDS-PAGE and detected with anti-GP2 antibody, 22.5D. (B) Cleavage efficiency and cell-to-cell fusion data. (C) Transduction of HAP1 and HAP1-ΔDAG1 cells using VSV pseudotyped particles. All data are based on the average and standard error of the mean of at least three replicate experiments.

Table 4.1. Summary of Fusion, GP cleavage and Transductions

Mutant	Classification	Fusion Activity	Cleavage Efficiency	Transduction Efficiency	
				HAP1	HAP1-ΔDAG
F262A	Hydrophobic	92.4 ± 17	106.6 ± 7	73.9 ± 13	96.7 ± 9
L266A	Hydrophobic	69.3 ± 17	86 ± 20	43.8 ± 15	70.1 ± 17
E270A	Charged	117.7 ± 13	123.9 ± 23	83.8 ± 8	65.9 ± 10
E272A	Charged	64.1 ± 22	112.5 ± 13	93.1 ± 7	78.9 ± 18
D273A	Charged	82.9 ± 6	103.4 ± 10	89.5 ± 7	56.8 ± 11
K300A	Charged	55.1 ± 26	86.4 ± 3	98.9 ± 6	95.6 ± 8
H305A	Charged	63.4 ± 18	88.8 ± 1	59.8 ± 15	34.7 ± 10
D306A	Charged	83.4 ± 13	80.1 ± 13	60.7 ± 15	56.6 ± 13
L313A	Hydrophobic	60.7 ± 21	98.7 ± 1	39.2 ± 9	38.3 ± 11
K320A	Charged	96 ± 9	101.5 ± 3	90.1 ± 3	55.2 ± 8
L326A	Hydrophobic	90 ± 5	70.4 ± 13	82.5 ± 15	74.3 ± 10
K327A	Charged	78.3 ± 9	89.8 ± 6	91.3 ± 6	79 ± 11
L349A	Hydrophobic	93.2 ± 8	99.9 ± 2	61.6 ± 15	61.6 ± 10
K352A	Charged	90.3 ± 11	57.8 ± 29	62.4 ± 19	70.7 ± 21
H354A	Charged	96.9 ± 4	87.6 ± 19	80.7 ± 7	68.9 ± 22
R356A	Charged	92.3 ± 14	78.3 ± 15	50.3 ± 24	37.7 ± 8
I358A	Hydrophobic	98.3 ± 5	103.3 ± 2	85.6 ± 14	77.4 ± 18
I361A	Hydrophobic	102.2 ± 24	103.9 ± 2	23.4 ± 10	24.4 ± 9
K384A	Charged	64.6 ± 1	49.2 ± 16	69.2 ± 4	52 ± 13
L387A	Hydrophobic	112.9 ± 29	102.2 ± 3	47.2 ± 10	40.6 ± 15
H398A	Charged	68.6 ± 33	80.6 ± 12	89.2 ± 5	52 ± 18
E404A	Charged	51.2 ± 13	97.1 ± 3	85.8 ± 10	58.3 ± 14
H448A	Charged	64.9 ± 3	115 ± 6	55.7 ± 27	31.8 ± 5
L449A	Hydrophobic	87.8 ± 11	91.2 ± 3	78.4 ± 14	70 ± 17
K451A	Charged	77.1 ± 12	109.8 ± 1	92.6 ± 6	79.4 ± 12
I458A	Hydrophobic	91.8 ± 8	103.4 ± 1	100.8 ± 19	82.6 ± 26
K461A	Charged	50.9 ± 7	103.2 ± 8	57.3 ± 18	21.4 ± 7
K465A	Charged	40.1 ± 11	110.6 ± 12	2.4 ± 1	23 ± 4
R481A	Charged	74.9 ± 2	141.3 ± 24	96.6 ± 9	91.1 ± 13
R490A-R491A	Charged	91.8 ± 7	138.3 ± 33	99.5 ± 5	82.3 ± 11

CHAPTER 5

CONCLUSION

The purpose of the work presented here was to identify amino acids within LASV GP1 required for αDG receptor binding and residues within GP2 required for protein functionality. In total, we characterized 140 constructs containing engineered mutations throughout the LASV GP. These constructs were biochemically tested for their ability to become processed, surface expressed, mediate cell-to-cell fusion, and transduce two different haploid cell lines. Mutations within the GP1 subunit, thought to be inhibiting αDG interactions, were also tested for their ability to bind αDG through co-immunoprecipitation.

Several conclusions on the domains and specific amino acid residues critical for LASV GP function have been reached through these studies. First, the αDG receptor binding site for OW arenaviruses is conserved. We, along with others, demonstrate that the αDG binding site for arenaviruses exists atop of the GP trimer (53). Experimental evidence suggests that the αDG binding site spans multiple GP1 monomers and requires an intact trimer because monomeric GP is unable to mediate αDG binding.

Secondly, we further supported regions within LASV GP1 required for LAMP1 interactions. Lassa virus is currently the only known arenavirus to require LAMP1 for efficient cellular entry. We and others demonstrated that the histidine triad within GP1 is important for mediating LAMP1 interactions (51, 61). Presumably the histidine triad indirectly affects LAMP1 binding through pH induced conformational changes. We also showed that insertional mutations near the LAMP1 binding crevice abolished transduction into both HAP1 and HAP1-DAG cells suggesting that these HA tag inserts interfere with LAMP1 interaction.

Lastly we have highlighted conserved residues within LASV GP2 required for mediating GP induced fusion by altering both hydrophobic and charged residues to alanine. We identified several residues within the GP2 fusion peptide, fusion loop and heptad repeats and some outside of these specified domains which alter GP2 function. Residues located in the fusion loop that negatively impacted fusion include L280, L285-I286, R282 and K291. These residues may help to position the fusion loop for insertion or could be directly involved in membrane insertion. Several other residues (I323, R355, I404, I411 and L415) located near or within the HR1 and HR2 domains of LASV GP2 also negatively affected fusion. These amino acids could be involved in 6HB formation to mediate virus-host membrane merger. Future experiments will be required to biochemically test these claims.

Ultimately, knowledge gained by these studies have answered several core questions about the LASV GP which the scientific community can utilize in future arenaviral exploration. By determining the αDG receptor binding domain on GP1, other groups can apply our data to design small molecules that competitively inhibit receptor interaction. The discovery of entry inhibitors against LASV GP would have a large impact on the medical treatment of the disease due to the current lack of available therapeutics.

Also, our work with the LASV GP2 subunit highlighted several residues involved in protein function. In the future, constructs resulting in fusion defects but still expressing near wild type levels of protein processing/expression will be assessed to identify where in the fusion process the mutation is disrupting. For instance, GP2 triggering results in the disassociation of the GP1 subunit. Therefore, to identify if the mutation is affecting glycoprotein triggering, we can develop experiments to assay for GP1 disassociation. If the mutated glycoprotein is able to trigger but is

still unable to mediate fusion, then we can assess if the mutation is inhibiting 6HB formation by utilizing native page. Taking these steps would give us a better understanding on GP2 functionality, highlight residues required for viral entry, and potentially aid in the future development of antiviral compounds that target regions required for GP2 function.

References

1. **Gara N, Ghany MG.** 2013. What the infectious disease physician needs to know about pegylated interferon and ribavirin. Clin Infect Dis **56:**1629-1636.

2. **Hansel TT, Kropshofer H, Singer T, Mitchell JA, George AJ.** 2010. The safety and side effects of monoclonal antibodies. Nat Rev Drug Discov **9:**325-338.

3. **Crowcroft NS, Meltzer M, Evans M, Shetty N, Maguire H, Bahl M, Gair R, Brink N, Lockwood D, Gregor S, Jones J, Nicoll A, Gopal R, Brown D, Bannister B.** 2004. The public health response to a case of Lassa fever in London in 2000. J Infect **48:**221-228.

4. **McCormick JB, Fisher-Hoch SP.** 2002. Lassa fever. Curr Top Microbiol Immunol **262:**75-109.

5. **Borio L, Inglesby T, Peters CJ, Schmaljohn AL, Hughes JM, Jahrling PB, Ksiazek T, Johnson KM, Meyerhoff A, O'Toole T, Ascher MS, Bartlett J, Breman JG, Eitzen EM, Jr., Hamburg M, Hauer J, Henderson DA, Johnson RT, Kwik G, Layton M, Lillibridge S, Nabel GJ, Osterholm MT, Perl TM, Russell P, Tonat K, Working Group on Civilian B.** 2002. Hemorrhagic fever viruses as biological weapons: medical and public health management. JAMA **287:**2391-2405.

6. **Coltart CE, Lindsey B, Ghinai I, Johnson AM, Heymann DL.** 2017. The Ebola outbreak, 2013-2016: old lessons for new epidemics. Philos Trans R Soc Lond B Biol Sci **372**.

7. **Regules JA, Beigel JH, Paolino KM, Voell J, Castellano AR, Hu Z, Munoz P, Moon JE, Ruck RC, Bennett JW, Twomey PS, Gutierrez RL, Remich SA, Hack HR,**

Wisniewski ML, Josleyn MD, Kwilas SA, Van Deusen N, Mbaya OT, Zhou Y, Stanley DA, Jing W, Smith KS, Shi M, Ledgerwood JE, Graham BS, Sullivan NJ, Jagodzinski LL, Peel SA, Alimonti JB, Hooper JW, Silvera PM, Martin BK, Monath TP, Ramsey WJ, Link CJ, Lane HC, Michael NL, Davey RT, Jr., Thomas SJ, r V-Z-GPSG. 2017. A Recombinant Vesicular Stomatitis Virus Ebola Vaccine. N Engl J Med **376:**330-341.

8. **Group PIW, Multi-National PIIST, Davey RT, Jr., Dodd L, Proschan MA, Neaton J, Neuhaus Nordwall J, Koopmeiners JS, Beigel J, Tierney J, Lane HC, Fauci AS, Massaquoi MBF, Sahr F, Malvy D.** 2016. A Randomized, Controlled Trial of ZMapp for Ebola Virus Infection. N Engl J Med **375:**1448-1456.

9. **Gunther S, Lenz O.** 2004. Lassa virus. Crit Rev Clin Lab Sci **41:**339-390.

10. **Ajayi NA, Ukwaja KN, Ifebunandu NA, Nnabu R, Onwe FI, Asogun DA.** 2014. Lassa fever - full recovery without ribavarin treatment: a case report. Afr Health Sci **14:**1074-1077.

11. **Stephenson EH, Larson EW, Dominik JW.** 1984. Effect of environmental factors on aerosol-induced Lassa virus infection. J Med Virol **14:**295-303.

12. **Olayemi A, Cadar D, Magassouba N, Obadare A, Kourouma F, Oyeyiola A, Fasogbon S, Igbokwe J, Rieger T, Bockholt S, Jerome H, Schmidt-Chanasit J, Garigliany M, Lorenzen S, Igbahenah F, Fichet JN, Ortsega D, Omilabu S, Gunther S, Fichet-Calvet E.** 2016. New Hosts of The Lassa Virus. Sci Rep **6:**25280.

13. **Monath TP, Newhouse VF, Kemp GE, Setzer HW, Cacciapuoti A.** 1974. Lassa virus isolation from Mastomys natalensis rodents during an epidemic in Sierra Leone. Science **185:**263-265.

14. **Grahn A, Brave A, Lagging M, Dotevall L, Ekqvist D, Hammarstrom H, Karlberg H, Lagerqvist N, Sansone M, Tegnell A, Ulleryd P, Studahl M.** 2016. Imported Case of Lassa Fever in Sweden With Encephalopathy and Sensorineural Hearing Deficit. Open Forum Infect Dis **3:**ofw198.

15. **Amorosa V, MacNeil A, McConnell R, Patel A, Dillon KE, Hamilton K, Erickson BR, Campbell S, Knust B, Cannon D, Miller D, Manning C, Rollin PE, Nichol ST.** 2010. Imported Lassa fever, Pennsylvania, USA, 2010. Emerg Infect Dis **16:**1598-1600.

16. **Atkin S, Anaraki S, Gothard P, Walsh A, Brown D, Gopal R, Hand J, Morgan D.** 2009. The first case of Lassa fever imported from Mali to the United Kingdom, February 2009. Euro Surveill **14**.

17. **Haas WH, Breuer T, Pfaff G, Schmitz H, Kohler P, Asper M, Emmerich P, Drosten C, Golnitz U, Fleischer K, Gunther S.** 2003. Imported Lassa fever in Germany: surveillance and management of contact persons. Clin Infect Dis **36:**1254-1258.

18. **Takei K, Haucke V.** 2001. Clathrin-mediated endocytosis: membrane factors pull the trigger. Trends Cell Biol **11:**385-391.

19. **Nabi IR, Le PU.** 2003. Caveolae/raft-dependent endocytosis. J Cell Biol **161:**673-677.

20. **Cureton DK, Massol RH, Saffarian S, Kirchhausen TL, Whelan SP.** 2009. Vesicular stomatitis virus enters cells through vesicles incompletely coated with clathrin that depend upon actin for internalization. PLoS Pathog **5:**e1000394.

21. **Helenius A, Kartenbeck J, Simons K, Fries E.** 1980. On the entry of Semliki forest virus into BHK-21 cells. J Cell Biol **84:**404-420.

22. **Pelkmans L, Kartenbeck J, Helenius A.** 2001. Caveolar endocytosis of simian virus 40 reveals a new two-step vesicular-transport pathway to the ER. Nat Cell Biol **3:**473-483.

23. **Kerr MC, Teasdale RD.** 2009. Defining macropinocytosis. Traffic **10:**364-371.

24. **Rojek JM, Sanchez AB, Nguyen NT, de la Torre JC, Kunz S.** 2008. Different mechanisms of cell entry by human-pathogenic Old World and New World arenaviruses. J Virol **82:**7677-7687.

25. **Oppliger J, Torriani G, Herrador A, Kunz S.** 2016. Lassa virus cell entry via dystroglycan involves an unusual pathway of macropinocytosis. J Virol doi:10.1128/JVI.00257-16.

26. **Aleksandrowicz P, Marzi A, Biedenkopf N, Beimforde N, Becker S, Hoenen T, Feldmann H, Schnittler HJ.** 2011. Ebola virus enters host cells by macropinocytosis and clathrin-mediated endocytosis. J Infect Dis **204 Suppl 3:**S957-967.

27. **Leonoudakis D, Huang G, Akhavan A, Fata JE, Singh M, Gray JW, Muschler JL.** 2014. Endocytic trafficking of laminin is controlled by dystroglycan and is disrupted in cancers. J Cell Sci **127:**4894-4903.

28. **Strecker T, Eichler R, Meulen J, Weissenhorn W, Dieter Klenk H, Garten W, Lenz O.** 2003. Lassa virus Z protein is a matrix protein and sufficient for the release of virus-like particles [corrected]. J Virol **77:**10700-10705.

29. **Pfau CJ.** 1996. Arenaviruses. *In* Baron S (ed), Medical Microbiology, 4th ed, Galveston (TX).

30. **Choppin PW, Scheid A.** 1980. The role of viral glycoproteins in adsorption, penetration, and pathogenicity of viruses. Rev Infect Dis **2:**40-61.

31. **Moulard M, Hallenberger S, Garten W, Klenk HD.** 1999. Processing and routage of HIV glycoproteins by furin to the cell surface. Virus Res **60:**55-65.

32. **Hallenberger S, Moulard M, Sordel M, Klenk HD, Garten W.** 1997. The role of eukaryotic subtilisin-like endoproteases for the activation of human immunodeficiency virus glycoproteins in natural host cells. J Virol **71:**1036-1045.

33. **Klenk HD, Garten W.** 1994. Host cell proteases controlling virus pathogenicity. Trends Microbiol **2:**39-43.

34. **Stieneke-Grober A, Vey M, Angliker H, Shaw E, Thomas G, Roberts C, Klenk HD, Garten W.** 1992. Influenza virus hemagglutinin with multibasic cleavage site is activated by furin, a subtilisin-like endoprotease. EMBO J **11:**2407-2414.

35. **Kido H, Yokogoshi Y, Sakai K, Tashiro M, Kishino Y, Fukutomi A, Katunuma N.** 1992. Isolation and characterization of a novel trypsin-like protease found in rat bronchiolar epithelial Clara cells. A possible activator of the viral fusion glycoprotein. J Biol Chem **267:**13573-13579.

36. **Skehel JJ, Wiley DC.** 2000. Receptor binding and membrane fusion in virus entry: the influenza hemagglutinin. Annu Rev Biochem **69:**531-569.

37. **Pager CT, Craft WW, Jr., Patch J, Dutch RE.** 2006. A mature and fusogenic form of the Nipah virus fusion protein requires proteolytic processing by cathepsin L. Virology **346:**251-257.

38. **Pager CT, Dutch RE.** 2005. Cathepsin L is involved in proteolytic processing of the Hendra virus fusion protein. J Virol **79:**12714-12720.

39. **Tashiro M, Yokogoshi Y, Tobita K, Seto JT, Rott R, Kido H.** 1992. Tryptase Clara, an activating protease for Sendai virus in rat lungs, is involved in pneumopathogenicity. J Virol **66:**7211-7216.

40. **Burri DJ, Pasqual G, Rochat C, Seidah NG, Pasquato A, Kunz S.** 2012. Molecular characterization of the processing of arenavirus envelope glycoprotein precursors by subtilisin kexin isozyme-1/site-1 protease. J Virol **86:**4935-4946.

41. **Kunz S, Edelmann KH, de la Torre JC, Gorney R, Oldstone MB.** 2003. Mechanisms for lymphocytic choriomeningitis virus glycoprotein cleavage, transport, and incorporation into virions. Virology **314:**168-178.

42. **Beyer WR, Popplau D, Garten W, von Laer D, Lenz O.** 2003. Endoproteolytic processing of the lymphocytic choriomeningitis virus glycoprotein by the subtilase SKI-1/S1P. J Virol **77:**2866-2872.

43. **Lenz O, ter Meulen J, Klenk HD, Seidah NG, Garten W.** 2001. The Lassa virus glycoprotein precursor GP-C is proteolytically processed by subtilase SKI-1/S1P. Proc Natl Acad Sci U S A **98:**12701-12705.

44. **Messina EL, York J, Nunberg JH.** 2012. Dissection of the role of the stable signal peptide of the arenavirus envelope glycoprotein in membrane fusion. J Virol **86:**6138-6145.

45. **Eichler R, Lenz O, Strecker T, Eickmann M, Klenk HD, Garten W.** 2003. Identification of Lassa virus glycoprotein signal peptide as a trans-acting maturation factor. EMBO Rep **4:**1084-1088.

46. **Bederka LH, Bonhomme CJ, Ling EL, Buchmeier MJ.** 2014. Arenavirus stable signal peptide is the keystone subunit for glycoprotein complex organization. MBio **5:**e02063.

47. **Agnihothram SS, York J, Trahey M, Nunberg JH.** 2007. Bitopic membrane topology of the stable signal peptide in the tripartite Junin virus GP-C envelope glycoprotein complex. J Virol **81:**4331-4337.

48. **York J, Nunberg JH.** 2006. Role of the stable signal peptide of Junin arenavirus envelope glycoprotein in pH-dependent membrane fusion. J Virol **80:**7775-7780.

49. **Briknarova K, Thomas CJ, York J, Nunberg JH.** 2011. Structure of a zinc-binding domain in the Junin virus envelope glycoprotein. J Biol Chem **286:**1528-1536.

50. **Hastie KM, Zandonatti MA, Kleinfelter LM, Heinrich ML, Rowland MM, Chandran K, Branco LM, Robinson JE, Garry RF, Saphire EO.** 2017. Structural basis for antibody-mediated neutralization of Lassa virus. Science **356:**923-928.

51. **Cohen-Dvashi H, Cohen N, Israeli H, Diskin R.** 2015. Molecular Mechanism for LAMP1 Recognition by Lassa Virus. J Virol **89:**7584-7592.

52. **Li S, Sun Z, Pryce R, Parsy ML, Fehling SK, Schlie K, Siebert CA, Garten W, Bowden TA, Strecker T, Huiskonen JT.** 2016. Acidic pH-Induced Conformations and LAMP1 Binding of the Lassa Virus Glycoprotein Spike. PLoS Pathog **12:**e1005418.

53. **Hastie KM, Igonet S, Sullivan BM, Legrand P, Zandonatti MA, Robinson JE, Garry RF, Rey FA, Oldstone MB, Saphire EO.** 2016. Crystal structure of the prefusion

surface glycoprotein of the prototypic arenavirus LCMV. Nat Struct Mol Biol doi:10.1038/nsmb.3210.

54. **Igonet S, Vaney MC, Vonrhein C, Bricogne G, Stura EA, Hengartner H, Eschli B, Rey FA.** 2011. X-ray structure of the arenavirus glycoprotein GP2 in its postfusion hairpin conformation. Proc Natl Acad Sci U S A **108:**19967-19972.

55. **Cao W, Henry MD, Borrow P, Yamada H, Elder JH, Ravkov EV, Nichol ST, Compans RW, Campbell KP, Oldstone MB.** 1998. Identification of alpha-dystroglycan as a receptor for lymphocytic choriomeningitis virus and Lassa fever virus. Science **282:**2079-2081.

56. **Shimojima M, Stroher U, Ebihara H, Feldmann H, Kawaoka Y.** 2012. Identification of cell surface molecules involved in dystroglycan-independent Lassa virus cell entry. J Virol **86:**2067-2078.

57. **Goncalves AR, Moraz ML, Pasquato A, Helenius A, Lozach PY, Kunz S.** 2013. Role of DC-SIGN in Lassa virus entry into human dendritic cells. J Virol **87:**11504-11515.

58. **Jae LT, Raaben M, Herbert AS, Kuehne AI, Wirchnianski AS, Soh TK, Stubbs SH, Janssen H, Damme M, Saftig P, Whelan SP, Dye JM, Brummelkamp TR.** 2014. Virus entry. Lassa virus entry requires a trigger-induced receptor switch. Science **344:**1506-1510.

59. **Jae LT, Raaben M, Riemersma M, van Beusekom E, Blomen VA, Velds A, Kerkhoven RM, Carette JE, Topaloglu H, Meinecke P, Wessels MW, Lefeber DJ, Whelan SP, van Bokhoven H, Brummelkamp TR.** 2013. Deciphering the glycosylome of dystroglycanopathies using haploid screens for lassa virus entry. Science **340:**479-483.

60. **Nunberg JH, York J.** 2012. The curious case of arenavirus entry, and its inhibition. Viruses **4:**83-101.

61. **Cohen-Dvashi H, Israeli H, Shani O, Katz A, Diskin R.** 2016. Role of LAMP1 Binding and pH Sensing by the Spike Complex of Lassa Virus. J Virol **90:**10329-10338.

62. **Israeli H, Cohen-Dvashi H, Shulman A, Shimon A, Diskin R.** 2017. Mapping of the Lassa virus LAMP1 binding site reveals unique determinants not shared by other old world arenaviruses. PLoS Pathog **13:**e1006337.

63. **Mellman I, Fuchs R, Helenius A.** 1986. Acidification of the endocytic and exocytic pathways. Annu Rev Biochem **55:**663-700.

64. **Cohen-Dvashi H, Israeli H, Shani O, Katz A, Diskin R.** 2016. The role of LAMP1 binding and pH sensing by the spike complex of Lassa virus. J Virol doi:10.1128/JVI.01624-16.

65. **White JM, Delos SE, Brecher M, Schornberg K.** 2008. Structures and mechanisms of viral membrane fusion proteins: multiple variations on a common theme. Crit Rev Biochem Mol Biol **43:**189-219.

66. **Welch BD, Liu Y, Kors CA, Leser GP, Jardetzky TS, Lamb RA.** 2012. Structure of the cleavage-activated prefusion form of the parainfluenza virus 5 fusion protein. Proc Natl Acad Sci U S A **109:**16672-16677.

67. **Allaway GP, Davis-Bruno KL, Beaudry GA, Garcia EB, Wong EL, Ryder AM, Hasel KW, Gauduin MC, Koup RA, McDougal JS, et al.** 1995. Expression and characterization of CD4-IgG2, a novel heterotetramer that neutralizes primary HIV type 1 isolates. AIDS Res Hum Retroviruses **11:**533-539.

68. **Moore JP, Sattentau QJ, Klasse PJ, Burkly LC.** 1992. A monoclonal antibody to CD4 domain 2 blocks soluble CD4-induced conformational changes in the envelope glycoproteins of human immunodeficiency virus type 1 (HIV-1) and HIV-1 infection of CD4+ cells. J Virol **66:**4784-4793.

69. **Kliger Y, Shai Y.** 2000. Inhibition of HIV-1 entry before gp41 folds into its fusion-active conformation. J Mol Biol **295:**163-168.

70. **Wild CT, Shugars DC, Greenwell TK, McDanal CB, Matthews TJ.** 1994. Peptides corresponding to a predictive alpha-helical domain of human immunodeficiency virus type 1 gp41 are potent inhibitors of virus infection. Proc Natl Acad Sci U S A **91:**9770-9774.

71. **Kilby JM, Hopkins S, Venetta TM, DiMassimo B, Cloud GA, Lee JY, Alldredge L, Hunter E, Lambert D, Bolognesi D, Matthews T, Johnson MR, Nowak MA, Shaw GM, Saag MS.** 1998. Potent suppression of HIV-1 replication in humans by T-20, a peptide inhibitor of gp41-mediated virus entry. Nat Med **4:**1302-1307.

72. **Chan DC, Kim PS.** 1998. HIV entry and its inhibition. Cell **93:**681-684.

73. **Chong H, Xue J, Xiong S, Cong Z, Ding X, Zhu Y, Liu Z, Chen T, Feng Y, He L, Guo Y, Wei Q, Zhou Y, Qin C, He Y.** 2017. A Lipopeptide HIV-1/2 Fusion Inhibitor with Highly Potent In Vitro, Ex Vivo, and In Vivo Antiviral Activity. J Virol **91**.

74. **Papp I, Sieben C, Ludwig K, Roskamp M, Bottcher C, Schlecht S, Herrmann A, Haag R.** 2010. Inhibition of influenza virus infection by multivalent sialic-acid-functionalized gold nanoparticles. Small **6:**2900-2906.

75. **Matsubara T, Onishi A, Saito T, Shimada A, Inoue H, Taki T, Nagata K, Okahata Y, Sato T.** 2010. Sialic acid-mimic peptides as hemagglutinin inhibitors for anti-influenza therapy. J Med Chem **53:**4441-4449.

76. **Rajik M, Omar AR, Ideris A, Hassan SS, Yusoff K.** 2009. A novel peptide inhibits the influenza virus replication by preventing the viral attachment to the host cells. Int J Biol Sci **5:**543-548.

77. **Jones JC, Turpin EA, Bultmann H, Brandt CR, Schultz-Cherry S.** 2006. Inhibition of influenza virus infection by a novel antiviral peptide that targets viral attachment to cells. J Virol **80:**11960-11967.

78. **Spence JS, Melnik LI, Badani H, Wimley WC, Garry RF.** 2014. Inhibition of arenavirus infection by a glycoprotein-derived peptide with a novel mechanism. J Virol **88:**8556-8564.

79. **Shankar S, Whitby LR, Casquilho-Gray HE, York J, Boger DL, Nunberg JH.** 2016. Small-Molecule Fusion Inhibitors Bind the pH-Sensing Stable Signal Peptide-GP2 Subunit Interface of the Lassa Virus Envelope Glycoprotein. J Virol **90:**6799-6807.

80. **Cashman KA, Smith MA, Twenhafel NA, Larson RA, Jones KF, Allen RD, 3rd, Dai D, Chinsangaram J, Bolken TC, Hruby DE, Amberg SM, Hensley LE, Guttieri MC.** 2011. Evaluation of Lassa antiviral compound ST-193 in a guinea pig model. Antiviral Res **90:**70-79.

81. **Whitby LR, Lee AM, Kunz S, Oldstone MB, Boger DL.** 2009. Characterization of lassa virus cell entry inhibitors: determination of the active enantiomer by asymmetric synthesis. Bioorg Med Chem Lett **19:**3771-3774.

82. **Frame JD, Baldwin JM, Jr., Gocke DJ, Troup JM.** 1970. Lassa fever, a new virus disease of man from West Africa. I. Clinical description and pathological findings. Am J Trop Med Hyg **19:**670-676.

83. **Mofolorunsho KC.** 2016. Outbreak of lassa fever in Nigeria: measures for prevention and control. Pan Afr Med J **23:**210.

84. **Fichet-Calvet E, Rogers DJ.** 2009. Risk maps of Lassa fever in West Africa. PLoS Negl Trop Dis **3:**e388.

85. **Ogbu O, Ajuluchukwu E, Uneke CJ.** 2007. Lassa fever in West African sub-region: an overview. J Vector Borne Dis **44:**1-11.

86. **Yun NE, Walker DH.** 2012. Pathogenesis of Lassa fever. Viruses **4:**2031-2048.

87. **Eichler R, Lenz O, Strecker T, Garten W.** 2003. Signal peptide of Lassa virus glycoprotein GP-C exhibits an unusual length. FEBS Lett **538:**203-206.

88. **York J, Nunberg JH.** 2007. A novel zinc-binding domain is essential for formation of the functional Junin virus envelope glycoprotein complex. J Virol **81:**13385-13391.

89. **Eschli B, Quirin K, Wepf A, Weber J, Zinkernagel R, Hengartner H.** 2006. Identification of an N-terminal trimeric coiled-coil core within arenavirus glycoprotein 2 permits assignment to class I viral fusion proteins. J Virol **80:**5897-5907.

90. **Ono N, Tatsuo H, Hidaka Y, Aoki T, Minagawa H, Yanagi Y.** 2001. Measles viruses on throat swabs from measles patients use signaling lymphocytic activation molecule (CDw150) but not CD46 as a cellular receptor. J Virol **75:**4399-4401.

91. **Radoshitzky SR, Longobardi LE, Kuhn JH, Retterer C, Dong L, Clester JC, Kota K, Carra J, Bavari S.** 2011. Machupo virus glycoprotein determinants for human transferrin receptor 1 binding and cell entry. PLoS One **6:**e21398.

92. **Robinson JE, Hastie KM, Cross RW, Yenni RE, Elliott DH, Rouelle JA, Kannadka CB, Smira AA, Garry CE, Bradley BT, Yu H, Shaffer JG, Boisen ML, Hartnett JN, Zandonatti MA, Rowland MM, Heinrich ML, Martinez-Sobrido L, Cheng B, de la Torre JC, Andersen KG, Goba A, Momoh M, Fullah M, Gbakie M, Kanneh L, Koroma VJ, Fonnie R, Jalloh SC, Kargbo B, Vandi MA, Gbetuwa M, Ikponmwosa O, Asogun DA, Okokhere PO, Follarin OA, Schieffelin JS, Pitts KR, Geisbert JB, Kulakoski PC, Wilson RB, Happi CT, Sabeti PC, Gevao SM, Khan SH, Grant DS, Geisbert TW, Saphire EO, Branco LM, Garry RF.** 2016. Most neutralizing human monoclonal antibodies target novel epitopes requiring both Lassa virus glycoprotein subunits. Nat Commun **7:**11544.

93. **Lefrancois L, Lyles DS.** 1982. The interaction of antibody with the major surface glycoprotein of vesicular stomatitis virus. I. Analysis of neutralizing epitopes with monoclonal antibodies. Virology **121:**157-167.

94. **Whitt MA.** 2010. Generation of VSV pseudotypes using recombinant DeltaG-VSV for studies on virus entry, identification of entry inhibitors, and immune responses to vaccines. J Virol Methods **169:**365-374.

95. **Imperiali M, Thoma C, Pavoni E, Brancaccio A, Callewaert N, Oxenius A.** 2005. O Mannosylation of alpha-dystroglycan is essential for lymphocytic choriomeningitis virus receptor function. J Virol **79:**14297-14308.

96. **Bonhomme CJ, Capul AA, Lauron EJ, Bederka LH, Knopp KA, Buchmeier MJ.** 2011. Glycosylation modulates arenavirus glycoprotein expression and function. Virology **409:**223-233.

97. **Eichler R, Lenz O, Garten W, Strecker T.** 2006. The role of single N-glycans in proteolytic processing and cell surface transport of the Lassa virus glycoprotein GP-C. Virol J **3:**41.

98. **Gallagher P, Henneberry J, Wilson I, Sambrook J, Gething MJ.** 1988. Addition of carbohydrate side chains at novel sites on influenza virus hemagglutinin can modulate the folding, transport, and activity of the molecule. J Cell Biol **107:**2059-2073.

99. **Tsuchiya E, Sugawara K, Hongo S, Matsuzaki Y, Muraki Y, Li ZN, Nakamura K.** 2002. Effect of addition of new oligosaccharide chains to the globular head of influenza A/H2N2 virus haemagglutinin on the intracellular transport and biological activities of the molecule. J Gen Virol **83:**1137-1146.

100. **Paal T, Brindley MA, St Clair C, Prussia A, Gaus D, Krumm SA, Snyder JP, Plemper RK.** 2009. Probing the spatial organization of measles virus fusion complexes. J Virol **83:**10480-10493.

101. **Zavorotinskaya T, Albritton LM.** 1999. A hydrophobic patch in ecotropic murine leukemia virus envelope protein is the putative binding site for a critical tyrosine residue on the cellular receptor. J Virol **73:**10164-10172.

102. **Apte-Sengupta S, Navaratnarajah CK, Cattaneo R.** 2013. Hydrophobic and charged residues in the central segment of the measles virus hemagglutinin stalk mediate transmission of the fusion-triggering signal. J Virol **87:**10401-10404.

103. **Bae Y, Kingsman SM, Kingsman AJ.** 1997. Functional dissection of the Moloney murine leukemia virus envelope protein gp70. J Virol **71:**2092-2099.

104. **Wang WK, Dudek T, Essex M, Lee TH.** 1999. Hypervariable region 3 residues of HIV type 1 gp120 involved in CCR5 coreceptor utilization: therapeutic and prophylactic implications. Proc Natl Acad Sci U S A **96:**4558-4562.

105. **Johnson DE, Ostrowski P, Jaumouille V, Grinstein S.** 2016. The position of lysosomes within the cell determines their luminal pH. J Cell Biol **212:**677-692.

106. **Cosset FL, Marianneau P, Verney G, Gallais F, Tordo N, Pecheur EI, ter Meulen J, Deubel V, Bartosch B.** 2009. Characterization of Lassa virus cell entry and neutralization with Lassa virus pseudoparticles. J Virol **83:**3228-3237.

107. **Klewitz C, Klenk HD, ter Meulen J.** 2007. Amino acids from both N-terminal hydrophobic regions of the Lassa virus envelope glycoprotein GP-2 are critical for pH-dependent membrane fusion and infectivity. J Gen Virol **88:**2320-2328.

108. **Andersen KG, Shapiro BJ, Matranga CB, Sealfon R, Lin AE, Moses LM, Folarin OA, Goba A, Odia I, Ehiane PE, Momoh M, England EM, Winnicki S, Branco LM, Gire SK, Phelan E, Tariyal R, Tewhey R, Omoniwa O, Fullah M, Fonnie R, Fonnie M, Kanneh L, Jalloh S, Gbakie M, Saffa S, Karbo K, Gladden AD, Qu J, Stremlau M, Nekoui M, Finucane HK, Tabrizi S, Vitti JJ, Birren B, Fitzgerald M, McCowan C, Ireland A, Berlin AM, Bochicchio J, Tazon-Vega B, Lennon NJ, Ryan EM, Bjornson Z, Milner DA, Jr., Lukens AK, Broodie N, Rowland M, Heinrich M, Akdag M, et al.** 2015. Clinical Sequencing Uncovers Origins and Evolution of Lassa Virus. Cell **162:**738-750.

109. **Kunz S.** 2009. Receptor binding and cell entry of Old World arenaviruses reveal novel aspects of virus-host interaction. Virology **387:**245-249.

110. **Sullivan BM, Emonet SF, Welch MJ, Lee AM, Campbell KP, de la Torre JC, Oldstone MB.** 2011. Point mutation in the glycoprotein of lymphocytic choriomeningitis virus is necessary for receptor binding, dendritic cell infection, and long-term persistence. Proc Natl Acad Sci U S A **108:**2969-2974.

111. **Sevilla N, Kunz S, Holz A, Lewicki H, Homann D, Yamada H, Campbell KP, de La Torre JC, Oldstone MB.** 2000. Immunosuppression and resultant viral persistence by specific viral targeting of dendritic cells. J Exp Med **192:**1249-1260.

112. **Kunz S, Sevilla N, Rojek JM, Oldstone MB.** 2004. Use of alternative receptors different than alpha-dystroglycan by selected isolates of lymphocytic choriomeningitis virus. Virology **325:**432-445.

113. **Teng MN, Borrow P, Oldstone MB, de la Torre JC.** 1996. A single amino acid change in the glycoprotein of lymphocytic choriomeningitis virus is associated with the ability to cause growth hormone deficiency syndrome. J Virol **70:**8438-8443.

114. **Smelt SC, Borrow P, Kunz S, Cao W, Tishon A, Lewicki H, Campbell KP, Oldstone MB.** 2001. Differences in affinity of binding of lymphocytic choriomeningitis virus strains to the cellular receptor alpha-dystroglycan correlate with viral tropism and disease kinetics. J Virol **75:**448-457.

115. **Aftabuddin M, Kundu S.** 2007. Hydrophobic, hydrophilic, and charged amino acid networks within protein. Biophys J **93:**225-231.

116. **Mindell JA.** 2012. Lysosomal acidification mechanisms. Annu Rev Physiol **74:**69-86.